# FINAL TECHNICAL REPORT

| | |
|---|---|
| **Project Title:** | Textures in Strip-Cast Aluminum Alloys: Their On-Line Monitoring and Quantitative Effects on Formability |
| **Covering Period:** | May 1, 2000 through April 30, 2003 |
| **Date of Report:** | July 27, 2003 |
| **Recipient:** | University of Kentucky Research Foundation<br>201 Kinkead Hall, Lexington, KY 40506-0057 |
| **Award Number:** | DE-FC07-00ID13902 |
| **Subcontractors:** | Industrial Materials Institute (IMI), National Research Council Canada<br>Katsuhiro Kawashima, Tokyo University of Technology, Japan |
| **Other Partners:** | Commonwealth Aluminum Corporation (CAC) |
| **Contact(s):** | Chi-Sing Man, (859) 257-3849, mclxyh@ms.uky.edu |
| **Project Team:** | DOE-HQ Program Manager: Thomas Robinson; Project Manager: John Yankeelov; Contract Specialist: Seb Klein; Industry Contact: Zhong Li (CAC) |

## Executive Summary

Aluminum sheets produced by continuous casting (CC) provide energy and economic savings of at least 25 and 14 percent, respectively, over sheets made from conventional direct chill (DC) ingot casting and rolling. As a result of the much simpler production route in continuous casting, however, the formability of CC aluminum alloys is often somewhat inferior to that of their DC counterparts. The mechanical properties of CC alloys can be improved by controlling their microstructure through optimal thermomechanical processing.

Suitable annealing is an important means to improve the formability of CC aluminum alloy sheets. Recrystallization of deformed grains occurs during annealing, and it changes the crystallographic texture of the aluminum sheet. Laboratory tests in this project showed that this texture change can be detected by either laser-ultrasound resonance spectroscopy or resonance EMAT (electromagnetic acoustic transducer) spectroscopy, and that monitoring this change allows the degree of recrystallization or the "recrystallized fraction" in an annealed sheet to be ascertained. Through a plant trial conducted in May 2002, this project further demonstrated that it is feasible to monitor the recrystallized state of a continuous-cast aluminum sheet in-situ on the production line by using a laser-ultrasound sensor. When used in conjunction with inline annealing, inline monitoring of the recrystallized fraction by laser-ultrasound resonance spectroscopy offers the possibility of feed-back control that helps optimize processing parameters (e.g., annealing temperature), detect production anomalies, ensure product quality, and further reduce production costs of continuous-cast aluminum alloys.

Crystallographic texture strongly affects the mechanical anisotropy/formability of metallic sheets. Clarification of the quantitative relationship between texture and anisotropy/formability of an aluminum alloy will render monitoring and control of its texture during the sheet production process even more meaningful. The present project included a study to determine how the anisotropic plastic behavior of a continuous-cast AA 5754 aluminum alloy depends on quantifiable texture coefficients. Formulae which show explicitly the effects of texture on the directional dependence of the $q$-value (a formability parameter) and of the uniaxial flow stress, respectively, were derived. Measurements made on a batch of as-received AA 5754 hot band and its O-temper counterpart corroborate the validity of these formulae. On the other hand, these measurements also indicate that some microstructure(s) other than texture could play a significant role in the plastic anisotropy of the AA 5754 alloy. For the $q$-value of a set of O-temper samples of this alloy, the additional microstructure that affects plastic anisotropy was shown to be grain shape. A formula that captures both the effects of crystallographic texture and grain shape on the $q$-value of the O-temper material was derived. A simple quadratic plastic potential that delivers this $q$-value formula was written down. Verification of the adequacy of this plastic potential, however, requires further investigations.

# Final Technical Report

As documented in the “Statement of Objectives” (DE-FC07-00ID13902 Amendment A000 Part III), the main objective of this project was “to determine whether laser-ultrasound resonance spectroscopy or resonance EMAT spectroscopy could be used to monitor texture, grain size, and thickness in selected strip-cast alloys on-line during hot rolling.” Also, “[s]ince monitoring of thickness should not be a problem, our R & D efforts will be focused on monitoring of texture and grain size.” A secondary objective of this project was “to develop a plastic potential, which adequately describes the forming characteristics of a selected strip-cast aluminum alloy at room temperature, and takes into account the effects of texture and grain size on its plastic flow behavior.” While the project activities stayed largely within the broad boundaries of the preceding statements, both objectives were modified to some extent during the course of this project. In what follows, the project activities and actual accomplishments under the two objectives are discussed in turn.

## On-Line Monitoring of Texture and Recrystallization

Under the first objective, the target in Year 1 was to determine whether laser-ultrasound resonance spectroscopy (LURS) or resonance EMAT (electromagnetic acoustic transducer) spectroscopy could be used in the laboratory to monitor texture and grain size in samples of a continuous-cast AA 5754 alloy at room temperature and at a selected set of elevated temperatures. The laser-ultrasound measurements were subcontracted to the Industrial Materials Institute (IMI), National Research Council Canada, whereas the EMAT measurements were subcontracted to Katsuhiro Kawashima, Tokyo University of Technology, Japan. Samples which had undergone various thermomechanical histories and were representative of a range of texture and grain-size conditions were sent to Canada and Japan for ultrasound measurements. At the University of Kentucky, X-ray and optical measurements were made on the samples to establish a data base on the textures and grain sizes versus the processing histories of the alloy in question. Soon it was realized that the grain size of samples of this alloy would remain almost unchanged for a broad range of processing conditions of interest to the aluminum industry. And, secondary recrystallization which would promote exaggerated grain growth could also be detected easily by monitoring the accompanying huge change in texture. Hence monitoring of grain size by measurement of ultrasound attenuation was dropped from the agenda of this project.

In summary, during Year 1 of this project, strong evidence was obtained which shows that the degree of primary recrystallization, grain growth, and secondary recrystallization of a continuous-cast AA 5754 alloy sheet can be monitored, at least under laboratory conditions and at temperatures up to 750 °F, by either resonance-EMAT or laser-ultrasound measurements of the velocity ratio $k$ , provided that the temperature of the sample in question is ascertained by another means. By definition the velocity ratio

$$k = \frac{V_L}{V_S}, \qquad (1)$$

where $V_L$ is the velocity of longitudinal wave propagating through the thickness of the sheet and $\overline{V_S}$ is the average of the two through-thickness shear-wave velocities.

Supported by results of Olsen cup and earing tests, we demonstrated that different annealing history did affect the formability of AA 5754 sheets differently. We singled out the texture coefficient $W_{400}$ as a good indicator for the degree of recrystallization and grain growth in the annealing of this AA 5754 alloy.

Theoretically we derived the formula

$$k = a(T) + b(T)W_{400}, \qquad (2)$$

where $a(T)$ and $b(T)$ are functions of the temperature $T$. Formula (2) was corroborated over a broad range of temperatures (unequivocally from room temperature to 600 °F, and likely also for the range from 600 °F to 750 °F) in laboratory measurements on AA 5754 samples, where $W_{400}$ was obtained from X-ray pole figures and $k$ was determined both by resonance EMAT spectroscopy and by laser-ultrasound resonance spectroscopy. The resonance-EMAT data on the functions $a(T)$ and $b(T)$ were well fitted by the formulae:

$$a(T) = 2.0246 + 1.189\times10^{-4}T + 8.14\times10^{-8}T^2, \quad b(T) = -3.569 - 1.740\times10^{-3}T, \qquad (3)$$

where the temperature $T$ is in °F. Hence we may monitor the degree of recrystallization by ultrasonic measurement of $k$. Repeated measurements of $k$ in short time intervals at 600 °F, 650 °F, and 700 °F, respectively, where recrystallization occurred in real time in the sample, when coupled with the $k$ versus temperature plots in our data, provide convincing evidence that supports the preceding assertion. More details about the resonance-EMAT measurements were reported in conference paper [6] listed in this report. A full length paper [5] on these findings is in preparation.

After these laboratory successes, a decision had to be made to select one of the two methods for a plant trial of inline measurements. Both methods had their strengths and weaknesses. From their collaborative work with the steel industry, IMI already had experience in building a laser-ultrasound prototype system for inline measurements. That the target sheet is moving and fluttering has no effect on laser-ultrasound measurements. On the other hand, unlike EMAT measurements, the generation laser in IMI's system left a discoloration marking each time it fired on the surface of the aluminum sheet. (IMI is currently developing another generation laser that might eliminate this problem altogether.) Moreover, the laser system was much less efficient than EMATs in generating shear waves, while the attenuation of shear waves in aluminum increases rapidly with temperature above 700 °F. As a result, the highest sample temperature at which resonance-EMAT measurement of texture could be made was shown in our laboratory study in Year 1 to be at least 850 °F, as compared with the maximum sensing temperature of about 380 °C (716 °F) for the IMI prototype system. But the EMAT method had its own problems. While non-contact, the EMAT sensor has to be kept very close (typically within 2 or 3 mm) to the sheet surface. This may cause a problem in inline

measurements where the aluminum sheet is moving and fluttering. As on-line applications of resonance-EMATs have been implemented in steel plants in Japan and Germany, there should be ways to overcome this difficulty, but the technical know-how is proprietary. Should the EMAT method be selected for plant trial in this project, it would require a development phase which might or might not be successful.

After consultations with our industrial partner Commonwealth Aluminum Corporation (CAC), we selected the method of laser-ultrasound resonance spectroscopy for plant trial and signed a subcontract with the Industrial Materials Institute (IMI), National Research Council Canada, for doing the on-line measurements. A plant trial on using laser-ultrasound resonance spectroscopy (LURS) for inline monitoring of texture and recrystallization in continuous-cast aluminum alloys was conducted at CAC's Carson Rolling Mill on May 2–3, 2002.

The plant trial on inline monitoring of texture and recrystallization by LURS was done in conjunction with the test runs of an inline induction furnace. While the annealing temperature of many test runs was set higher than the laser-ultrasound sensor's capabilities (maximum sensing temperature at about 380 °C or 716 °F), there were several runs at sufficiently low annealing temperatures that clear evidence of recrystallization and its effect on $k$ was recorded by the sensor. Since a cost effective processing line should set the annealing temperature as low as possible, we can say that the plant trial of inline monitoring of texture and recrystallization by LURS was a success. Details about the plant trial are given in an IMI report by André Moreau et al., which is attached to this report as an Appendix.

## Effects of Crystallographic Texture and Grain Shape on Plastic Anisotropy of Continuous-Cast AA 5754 Aluminum Alloy

As mentioned in the "Statement of Objectives", it was expected that this part of the project would be assigned to a graduate student as thesis research. Indeed, much of the experimental work reported below was done mainly by Ms. Yu Xiang as part of her dissertation research.

The approach that we followed was in part dictated by a handicap, namely that at the University of Kentucky we did not have a biaxial testing machine at our disposal. Thus the mechanical tests that we did were restricted to uniaxial tension tests. Measurements of the directional dependence of the *r*-value and of uniaxial flow stress served as the empirical basis for our investigations on plastic anisotropy. Also, for the same reason given in the first paragraph of the preceding section, effects of grain size on plastic flow were not investigated.

Investigations in this part of the project went through three stages:

1. Assuming that the plastic flow of a sheet metal is governed by a plastic potential whose anisotropic part depends linearly on the texture coefficients, Man [3] derived an expression which describes how crystallographic texture affects the angular dependence of the $r$-value in orthorhombic sheets of cubic metals. Similarly, a parallel expression was derived [8] for the angular dependence of the uniaxial flow stress $s$, provided that this dependence is determined by a yield function whose anisotropic part is linear in the texture coefficients. The derivations of these expressions require only that the plastic potential and the yield function be sufficiently smooth. Both expressions include terms

with texture coefficients $W_{lmn}$ for as large an $l$ as one cares to compute. Moreover, each formula contains material parameters other than texture coefficients (see, for example, Eq. (5) below).

2. Uniaxial tension tests were conducted [7] on samples of an as-received AA 5754 hot band and its O-temper counterpart. It was shown that, by a judicious choice of the undetermined parameters for each temper, Man's formulae truncated at $l = 6$ could fit [7] the experimental data well. The parameters obtained from the empirical fittings, however, were quite different for the two temper conditions. Our interpretation was that the differences in the fitting parameters reflect the effect of some other microstructure(s) on plastic anisotropy.
3. Work was initiated [9, 11] in Year 3 to find out what other microstructure(s) could play a significant role in the plastic anisotropy of the AA 5754 alloy and to delineate quantitatively their effect. For the O-temper material, empirical evidence indicated grain shape as the other microstructure at work. A formula incorporating both the effects of crystallographic texture and grain shape on the $q$-value, where $q = r/(r+1)$, was derived.

In what follows, we shall mainly discuss the latest work [10] on the O-temper material, which will also illustrate in passing some of the work in the earlier stages. Henceforth we always adopt a spatial Cartesian coordinate system such that the 1-, 2- and 3-direction agrees with the rolling (RD), transverse (TD) and normal direction (ND) of the sheet, respectively. We choose a reference orientation for the crystallites such that the spatial coordinate axes are axes of four-fold rotational symmetry of the reference cubic crystal. Let $q$ be the angle between the axis of the tension test coupon and the rolling direction of the metal sheet. In terms of $q = r/(r+1)$, when we keep only terms linear in the texture coefficients $W_{lmn}$ with $l \le 5$, Man's original expression [3] for orthorhombic sheets of cubic metals reduces to the form:

$$q = \frac{1}{2} + b_1(s)\left( W_{400} - \frac{2\sqrt{10}}{5} W_{420} \cos 2q - \frac{\sqrt{70}}{5} W_{440} \cos 4q \right). \tag{4}$$

When terms linear in $W_{lmn}$ up to $l = 7$ are kept, the expression assumes the form:

$$\begin{aligned} q = \frac{1}{2} &+ b_1(s)\left( W_{400} - \frac{2\sqrt{10}}{5} W_{420} \cos 2q - \frac{\sqrt{70}}{5} W_{440} \cos 4q \right) \\ &+ b_2(s)\left( W_{600} - \frac{17\sqrt{105}}{105} W_{620} \cos 2q + \frac{\sqrt{14}}{7} W_{640} \cos 4q + \frac{\sqrt{231}}{7} W_{660} \cos 6q \right). \end{aligned} \tag{5}$$

In Eqs. (4) and (5), $b_i(s)$ are functions of the uniaxial flow stress $s$ when the $q$-value measurement is made.

Table 1: Texture Coefficients of AA 5754 Hot Band and O-Temper Samples

| | $W_{400}$ | $W_{420}$ | $W_{440}$ | $W_{600}$ | $W_{620}$ | $W_{640}$ | $W_{660}$ |
|---|---|---|---|---|---|---|---|
| HB | $-0.0033$ | $-0.0025$ | $-0.0071$ | $-0.0048$ | $0.0062$ | $-0.0032$ | $-0.0011$ |
| O | $0.0072$ | $-0.0019$ | $0.0022$ | $0.0004$ | $0.0007$ | $-0.0017$ | $0.0004$ |

In Year 2 of this project, measurements were made [7] on samples of a continuous-cast AA 5754 aluminum hot band and its fully-annealed O-temper counterpart to examine the validity of Eqs. (4) and (5). The textures of the two mother sheets were measured by X-ray diffraction. The relevant texture coefficients are reported in Table 1.

For each angle $q$ of 0°, 15°, 30°, 45°, 60°, 75°, and 90°, two uniaxial tension test specimens were cut from each mother sheet. The experimental angular dependence of $q$-value was determined on these 28 specimens. Eq. (4) gave a good fit of the experimental data on the O-temper material but at best provided only a qualitative representation of the data on the hot band. Eq. (5) fit well the experimental data on the $q$-value of both materials. However, for the two hardness conditions of the aluminum alloy, it delivered very different values for the material parameters $b_i$ (which were found to be constant over the range of flow stress in the experiments), namely: $b_1 = -9.2$, $b_2 = 11.3$ for the hot band and $b_1 = -20.9$, $b_2 = 4.7$ for the O-temper sheet. This finding suggests that some aspect of the sample's microstructure, other than crystallographic texture, is also at work.

Since the O-temper aluminum alloy possessed nearly equiaxed grains in contrast to elongated grains in the hot band, it is natural to ask whether and how grain shape affects the anisotropy of the $q$-value in these materials. In Year 3 of this project, Eqs. (4) and (5) on the $q$-value were extended so that they would account also for the effect of grain shape.

Grain shape is described by the mean linear intercept function $f$ defined on the unit sphere. For a unit vector $\boldsymbol{n}(Y, Q)$, where $(Y, Q)$ are the spherical coordinates of $\boldsymbol{n}$, $f(\boldsymbol{n})$ is defined by the first expression and is approximately given by the second expression below:

$$f(\boldsymbol{n}) = \frac{1}{L^2(\boldsymbol{n})} \approx \boldsymbol{n} \bullet \boldsymbol{M}\boldsymbol{n}, \tag{6}$$

where $L(\boldsymbol{n})$ is the mean length of all line segments parallel to $\boldsymbol{n}$, each of which subtends some grain, and $\boldsymbol{M}$ is a second-order fabric tensor sometimes called the "Microstructural Anisotropy Tensor". We assume that $\boldsymbol{M}$ is orthorhombic with its symmetry axes agreeing with RD, TD, and ND. Let $s_1$, $s_2$, and $s_3$ be the eigenvalues of the deviatoric part of $\boldsymbol{M}$. Assuming that both the effects of grain shape and of crystallographic texture on the $q$-value be small, we derive [11] the following extension of Eq. (4):

$$q = \frac{1}{2} + b\left(s\,,\,\mathrm{tr}\,\boldsymbol{M}\right)\left(-3\left(s_1 + s_2\right) + \left(s_1 - s_2\right)\cos 2q\right)$$
$$+ b_1\left(s\,,\,\mathrm{tr}\,\boldsymbol{M}\right)\left(W_{400} - \frac{2\sqrt{10}}{5}W_{420}\cos 2q - \frac{\sqrt{70}}{5}W_{440}\cos 4q\right). \tag{7}$$

In Figure 1, we present the measured and predicted angular dependence of the $q$-value for the AA 5754 hot band and its O-temper counterpart. The discrete data points are experimental $q$-values reported in [7], whereas the dashed line gives the $q$-values as predicted by Eq. (4) and the solid line is the best-fit based on Eq. (7). Clearly Eq. (7), which includes also the effect of grain shape, fits the experimental data much better. However, it should be mentioned that in the fittings there is only one adjustable parameter in Eq. (4) but there are three for Eq. (7), a fact which will be discussed in more detail below.

Another interesting finding in this work is that the material parameters $b_i$ in Man's formula, which assume [6] very different values for the AA 5754 hot band and its O-temper counterpart under Eq. (5), now have much closer values under the new formula (7). The values of material parameter $b_1$ in Eq. (4) and Eq. (7) that best fit the measured $q$-value data are listed in Table 2.

When we did the least-square fitting, the term $b\left(s\,,\,\mathrm{tr}\,\boldsymbol{M}\right)\left(-3\left(s_1 + s_2\right) + \left(s_1 - s_2\right)\cos 2q\right)$ in Eq. (7) was written as the sum of $c$ and $d\cos 2q$, where

$$c = -3b\left(s\,,\,\mathrm{tr}\,\boldsymbol{M}\right)\left(s_1 + s_2\right), \qquad d = b\left(s\,,\,\mathrm{tr}\,\boldsymbol{M}\right)\left(s_1 - s_2\right),$$

and we allowed $c$ and $d$ to change as free parameters. Hence, the better fitting by the new

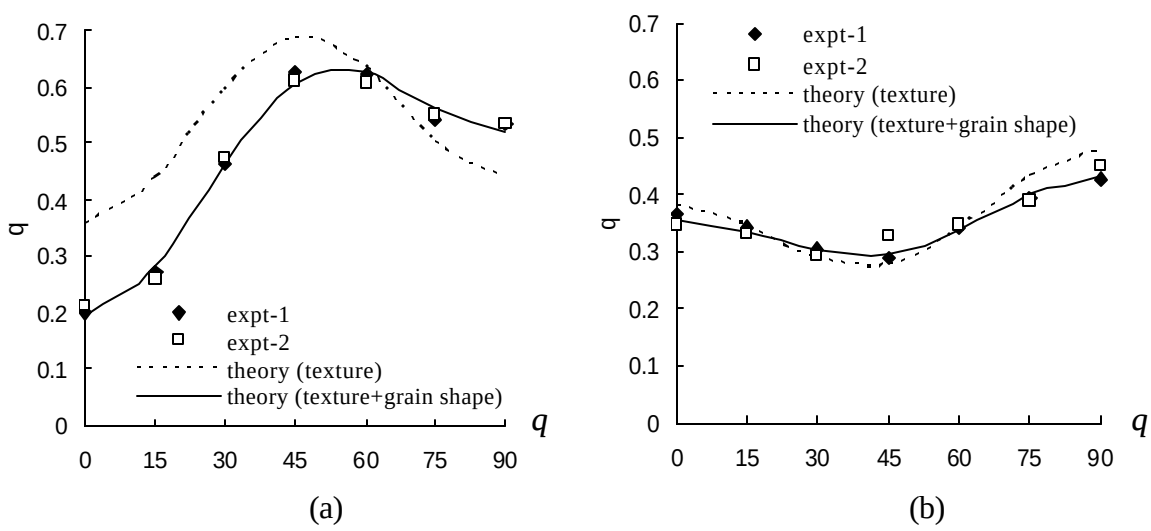


Figure 1: Plots of angular dependence of the $q$-value of an AA 5754 aluminum alloy (a) Hot band; (b) O-temper.

Table 2: Best-fit coefficients in Eq. (4) and Eq. (7) for $q$-value

| | $b_1$, Eq. (4) texture ($W_{4m0}$) | $b_1$, Eq. (7) texture ($W_{4m0}$) + grain shape |
|---|---|---|
| HB | $-12.2$ | $-10.5$ |
| O | $-20.7$ | $-12.8$ |

formula may be suspected because of the two additional free parameters. However, the closer values of $b_1$ for the hot band and its O-temper counterpart as delivered by Eq. (7) support the new formula, and the relation

$$\frac{c}{d} = \frac{-3(s_1 + s_2)}{(s_1 - s_2)} \tag{8}$$

allows a comparison between the ratio $c/d$ (as obtained from fitting) and the experimentally measured ratio $-3(s_1 + s_2)/(s_1 - s_2)$ to further verify Eq. (7).

For the O-temper material, the best fitting parameters *c* and *d* of Eq. (7) were 0.063 and 0.008, respectively, which yielded the ratio $c/d = 7.88$. The experimental $s_1$ and $s_2$ values were $-0.00024$ and $-0.00050$, respectively (see [11] for details); then $-3(s_1 + s_2)/(s_1 - s_2) = 8.41$.

Considering errors introduced in experimental determination of texture, $q$-value, $s_1$ and $s_2$, we regard the measured ratio (i.e., the right-hand side of Eq. (8)) as consistent with the value predicted by Eq. (7) from fitting of the $q$-value. This agreement suggests that Eq. (7) adequately describes the effects of texture and grain shape on the *q*-value of the O-temper sample.

It is easy to write down a quadratic plastic potential which delivers Eq. (7) as the angular dependence formula for the $q$-value. Verification of the adequacy of this plastic potential, however, requires further investigations (e.g., by biaxial mechanical tests).

While our measurements have corroborated Eq. (7) in the case of the O-temper sample, we can *not* conclude at this moment that Eq. (7) applies to the AA 5754 hot band, let alone to other aluminum alloys. Improvement of fitting of angular dependence of the $q$-value by adding an expression of the form $c + d\cos 2q$ in Eq. (4) need not indicate an effect of grain shape at the optical micro-level. Another microstructure (e.g., sub-grains) may lead to the same expression in the $q$-value formula so long as its influence on plastic anisotropy is realized through a second order tensor such as $\boldsymbol{M}$. Further experimental studies are in progress to examine the validity of Eq. (7) for more aluminum alloys; these studies include investigations on the possible roles of sub-grains and dislocation cells.

**Journal Publications:**


1. C.-S. Man and M. Huang, “Identification of material parameters in yield functions and flow rules for weakly-textured sheets of cubic metals", *International Journal of Non-Linear Mechanics* **36**, 501–514 (2001).
2. W.C. Liu, C.-S. Man, and J.G. Morris, “Lattice rotation of the cube orientation to the $b$ fiber during cold rolling of AA 5052 aluminum alloy", *Scripta Materialia* **45**, 807–814 (2001).
3. C.-S. Man, “On the $r$ -value of textured sheet metals”, *Int. J. Plasticity* **18**, 1683–1706 (2002).
4. W.C. Liu, T. Zhai, C.-S. Man, and J.G. Morris, “Quantification of recrystallization texture evolution in cold rolled AA 5182 aluminum alloy”, *Scripta Materialia*, in press.
5. C.-S. Man, X. Fan, J.G. Morris, and K. Kawashima, “Monitoring of texture and recrystallization in aluminum alloy by resonance EMAT spectroscopy”, to be submitted to *J. Appl. Phys.*


**Conference Papers:**


6. C.-S. Man, X. Fan, J.G. Morris, and K. Kawashima, “Monitoring of primary recrystallization in aluminum alloy by resonance EMAT spectroscopy”, *Materials Science Forum*, vol. 408–412, pp. 875–880 (2002).
7. C.-S. Man, Y. Zhang, and Y. Xiang, “Effects of crystallographic texture on plastic anisotropy of aluminum and titanium sheets”, in *Plasticity, Damage and Fracture at Macro, Micro and Nano Scales*, A.S. Khan and O. Lopez-Pamies (eds.), Neat Press, Fulton, Maryland, 2002, pp. 251–253.
8. C.-S. Man, “Flow stress anisotropy in textured sheet metals”, in *Proceedings of the Fourth International Conference on Nonlinear Mechanics* (Shanghai, August 13-16, 2002), Chien Wei-zang et al. (eds.), Shanghai University Press, Shanghai, China, 2002, pp. 98–101.
9. Y. Xiang and C.-S. Man, “Effect of texture and microstructure on plastic anisotropy of aluminum sheet”, in *Modeling the Performance of Engineering Structural Materials III,* D. Lesuer, T.S. Srivatsan, and E. Taleff (eds.), TMS, Warrendale, PA, 2002, pp. 323–331.
10. W.C. Liu, Z. Li. T. Zhai, C.-S. Man, and J.G. Morris, “Development of through-thickness texture gradient during continuous cast processing of AA 5052 aluminum alloy”, in *Hot Deformations of Aluminum Alloys III*, Z. Jin et al. (eds.), TMS, Warrendale, PA, 2003, pp. 125–134.
11. Y. Xiang and C.-S. Man, “Effects of grain shape and crystallographic texture on plastic anisotropy of aluminum alloy”, submitted to *Metallurgical Modeling for Aluminum Alloys*, M. Tiryakioglu (ed.).

# *Appendix:*

# *Inline Measurements of Texture and Recrystallization at Commonwealth Aluminum Corporation*

André Moreau, Christophe Bescond, Stéphane Bolognini, Martin Lord, Silvio Kruger

Characterization and Ultrasonic Sensors
Industrial Materials Institute
National Research Council Canada

2 April 2003; minor revisions, 23 July 2003

## Table of Contents

Inline Measurements of Texture and Recrystallization at Commonwealth Aluminum Corporation .....11

I Introduction .....13
- Project objectives .....13
- Executive summary.....13
- Report outline .....14

II Pyrometry .....15
- Introduction .....15
- Thermocouple.....15
- Multi-color pyrometer.....15
- IR camera .....17
- Comparison of the Williamson pyrometer and the IR camera data.....20
- Temperature drop from the pyrometer to the laser-ultrasound measurement point.20

III Laser-ultrasonic measurements and discussion .....23
- Laser-ultrasound resonance spectroscopy, texture, and recrystallization .....23
- Laser-ultrasound prototype description.....23
- Description of data analysis .....24
- Inline laser-ultrasonic measurements .....27
- Measurement limit, validity and accuracy.....39
- Supporting laser-ultrasonic measurements in the laboratory.....41
- Laser-ultrasonic attenuation and recrystallization .....46
- Using longitudinal resonances and a thickness gauge .....47

IV Practical considerations for inline LURS measurement of recrystallization.....49
- Introduction .....49
- Limitations of inline annealing.....49
- Inline monitoring of the recrystallized fraction.....50
- Limitations of inline monitoring of the recrystallized fraction: .....50
- Designing a processing line that includes a LUS sensor .....52
- Other benefits .....53
- Total savings.....53

V Conclusion.....54
- Recalling the objectives.....54
- The future .....54

VI Appendix I – Basic data for samples taken inline at CAC .....55

VII Appendix II – X-ray texture data for samples taken inline at CAC .....56

VIII Appendix III – Suppliers of laser-ultrasonic equipment. .....59

IX References .....60

# *I Introduction*

## Project objectives

The goal of this project is to determine whether 1) aluminum sheets can be fully recrystallized using an induction furnace after hot rolling and whether 2) recrystallization can be monitored inline with a laser-ultrasound sensor.

Commonwealth Aluminum Corporation desires to develop a continuous annealing process using an induction furnace. Such a process would replace batch annealing, reduce energy consumption, capital investments, and processing costs, and improve product uniformity. In addition, a laser-ultrasound sensor is being developed to provide an accurate measurement of the annealing state. This information would insure processing quality and could be applied in a feedback loop to better control furnace power, line speed, or other process parameters.

## Executive summary

In this report, inline tests of the laser-ultrasound sensor are reviewed and partly analyzed, with the aim to provide an answer to the second project objective.

A laser-ultrasound prototype system was built between September 2001 and March 2002 to measure the crystallographic texture of aluminum strips. The strip texture is modified by recrystallization, as described in previous work. The sensor is based on laser-ultrasound resonance spectroscopy (LURS). In summary, the sensor measures resonance frequencies of longitudinal and shear ultrasonic waves in the thickness of the strip. The ratio $k$ of these resonances is insensitive to thickness variations and varies with crystallographic texture and temperature. The temperature is also measured inline. Its effect on the resonance frequencies is known and can be removed from the data. Finally, $k$ is used to infer texture variations and, consequently, the recrystallization state of the strip.

The induction furnace and laser-ultrasound prototype sensor were tested inline at Commonwealth Aluminum Corporation (CAC) on May 2 and 3, 2002. The laser-ultrasound sensor performed as well in the plant as it did in the laboratory. The main difficulty, which we were aware of prior to the tests, is the large decrease in the shear signal amplitude with increasing temperature. Another difficulty arose from the failure of the pyrometer used to measure temperature. As a consequence, all temperature measurements were approximate only.

The data analysis shows that thickness variations are important and that the ratio $k$ of two resonances must be used to eliminate these variations. Evidence of recrystallization and its effect on $k$ was sensed approximately four seconds after inline annealing to 380 °C (716 °F). This temperature is near the limit of the sensor's capabilities to measure shear waves (380 °C, or 716 °F) but the temperature of the strip had cooled by approximately 20 °C (35 °F) in those four seconds between the furnace and the sensor so that the temperature at the sensor was approximately 360 °C, only. Further improvements to the sensor would raise this maximum sensing temperature by perhaps 10 to 70 degrees Celsius. However this may not be required:

In our opinion, a cost effective processing line would include a temperature holding time period where the strip would be given time to recrystallize. The longer this holding time would be, the lower would be the reheat temperature, and the greater would be the energy savings. In addition, just as during the tests at CAC, one could let the strip cool by perhaps another 20 °C after recrystallization and before the inline measurement. Therefore, given the multiplicity of potential solutions to this limitation, it should be relatively easy to install the sensor at a location where the high temperature limit of the sensor would be high enough to meet production requirements.

In conclusion, the laser-ultrasound sensor performed as well in the plant as it did in our laboratory and could sense recrystallization inline, in the relatively unfavourable conditions of the trial.

**Report outline**

Section II of this report is a detailed description of the temperature measurements. The essential information is that, because the main pyrometer failed, we had to rely on an inaccurate temperature measurement provided by an infrared camera. This section may be skipped.

Section III details the laser-ultrasonic measurements and data analysis. It is the core of the report.

Section IV is the authors' view on the best way to use the laser-ultrasonic sensor for maximum benefits. This section is self-contained and does not require an in-depth understanding of the sensor's working principles.

Following the Conclusion, some raw data are collected in the Appendices.

## *II Pyrometry*

### Introduction

Accurate temperature measurements are necessary because the recrystallization kinetics strongly depends on temperature and because the elastic properties to be measured using laser-ultrasound depend not only on texture but also on temperature. Three means were employed to measure temperature: a thermocouple in contact with the strip, a three-color pyrometer located at the exit of the furnace, and an infrared (IR) camera imaging almost the entire strip between the furnace and the coiler.

### Thermocouple

A thermocouple was used as a backup system and as a means to verify whether the pyrometer and IR camera worked reasonably well. This probe has four wheels that contact the Al sheet and maintain the sensing element at a constant height above the sheet. The sensing element is located between the four wheels. It is a thin metal foil that is nearly horizontal and bent in an arc shape. The middle of the arc contacts the Al sheet and presumably comes into thermal equilibrium with the sheet. A thermocouple located on the opposite side of the foil provides a temperature measurement. The thermocouple was located just after the pyrometer (perhaps within 1 meter), which was itself located near the exit of the furnace.

Although thermocouples usually provide excellent temperature measurements and are very reliable, in this case it is not clear that this is so. The contact between the probe and the moving sheet may not have been always good and friction between the Al sheet and the probe foil may have raised the temperature of the foil. Finally, the thermocouple was read intermittently by an operator who yelled the value to someone else who would record it. This process was slow and provided only a few measurements per coil. The magnitude of the temperature measurement errors was not estimated. The maximum stable sheet temperature recorded using the thermocouple for each trial is noted in Table I of Appendix I.

### Multi-color pyrometer

A Williamson Pro #120-25 multi-color pyrometer was selected among others because it claims to be most accurate for Al (accuracy of ± 0.5% of reading or ± 2 °C, repeatability better than 1 °C, according to the manufacturer's specifications). It was mounted vertically above the sheet, approximately 4 feet away from the exit of the induction furnace. The pyrometer signal was transmitted to a console where the temperature value was displayed together with other data such as line speed. An analog signal (DC current) proportional to temperature was then transmitted along a shielded twisted pair to one of IMI's computers where it was recorded. This cable ran too close to the induction furnace and captured too much electromagnetic noise. As a consequence, the values recorded by IMI are unusable. Only the values recorded by CAC using the console are used in this report.

The pyrometer seemed to operate well during the first measurement day, but it did not work at all during the second day. It appears that it was damaged during one of the sheet melt down incidents (too much power was applied to the induction furnace and the sheet was heated above its melting point). Figure 1 shows the temperature profile of coil 5754-3 as a function of time. This profile is selected because it displays the longest plateau at constant temperature. Figure 2 is the same profile but the temperature scale is magnified in the 800 to 900 °F region. The region between 60 and 90 seconds has a mean temperature of 869 °F with a standard deviation of ± 3 °F. This standard deviation reflects the combined true temperature variations of the aluminum sheet and the repeatability of the pyrometer measurements. Therefore, the

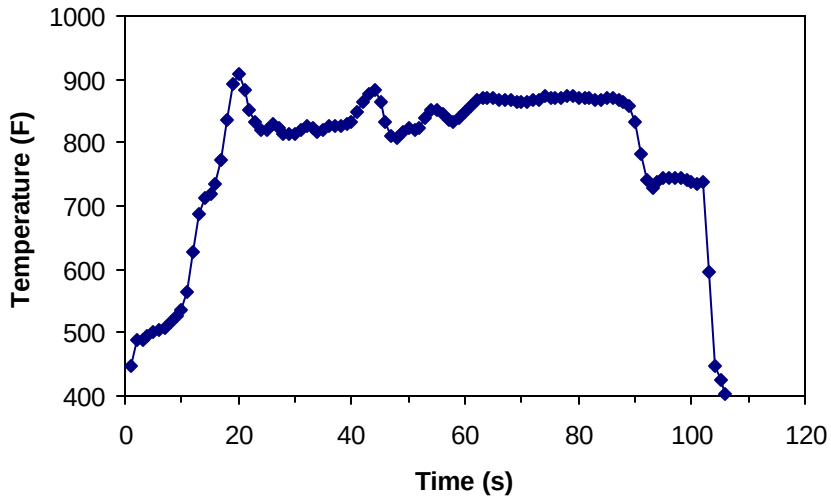


**Figure 1.** Temperature profile along the centerline of coil 5754-3 as measured with the Williamson pyrometer.

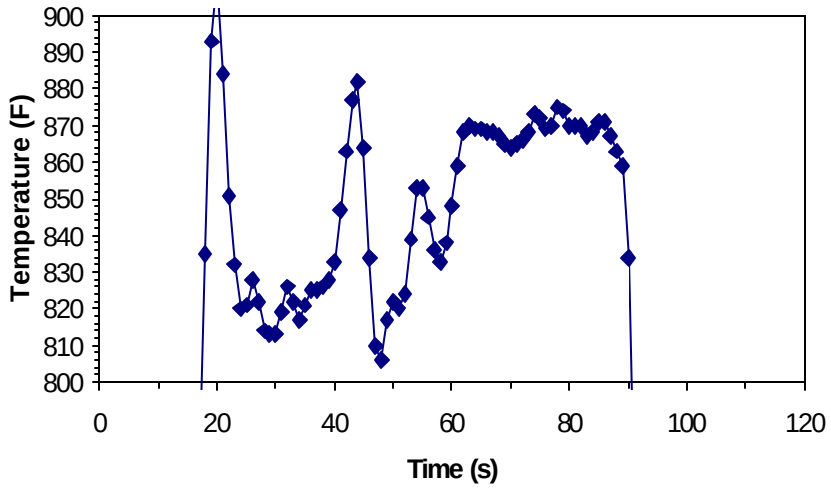


**Figure 2.** Enlargement of the temperature plateau observed in Fig. 1.

pyrometer's repeatability is better or equal to ± 3 °F. This provides a crude verification of the manufacturer's repeatability specification of ± 1 °C. It also makes us believe that larger variations, such as those observed between 20 and 60 seconds, are real. Finally, Table I shows that the highest (stable) temperature measured using the thermocouple and presumably the temperature of the plateau was 875 °F. Again, this agrees with the pyrometer value of 869 °F to within about twice the specifications of the pyrometer.

Figure 3 shows a graph of pyrometer vs. thermocouple temperature measurements. Clearly, the agreement is not nearly as good as for sample 5754-3. Because the thermocouple measurements are more prone to errors and because the pyrometer readings were made sporadically, perhaps once every few seconds at best (depending on the coil), we prefer the pyrometer values to the thermocouple values.

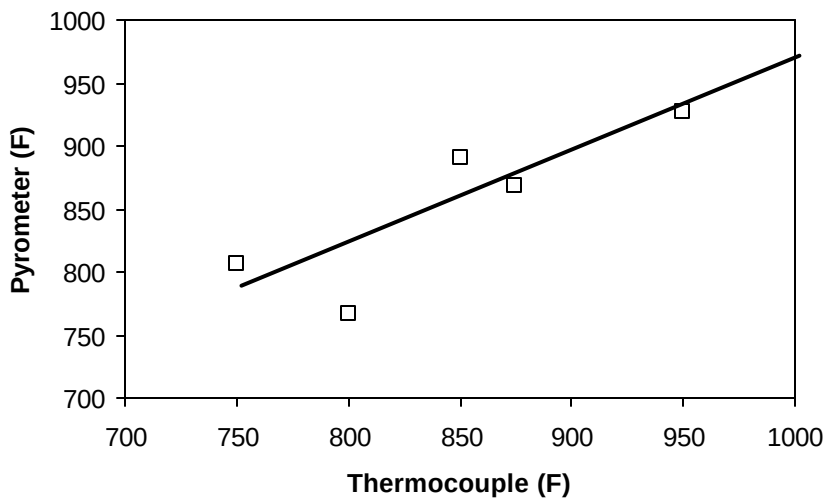


**Figure 3.** Pyrometer vs. thermocouple temperature measurements.

### IR camera

An infrared (IR) camera, working in the 8 to 12 $m$ m bandwidth, was used to image the strip and estimate the temperature drop between the pyrometer and the laser-ultrasonic sensor. The camera was located roughly 4 m (12 feet) above the floor level and looked down at the strip at an angle of 27 degrees. Because the strip was not horizontal but angled by a few degrees, and because of the wide viewing angle (40 degrees horizontally, 20 degrees vertically), the actual angle of the camera with respect to the sheet plane differed somewhat from 27 degrees. A typical IR image is shown in Fig. 4.

To block reflections from windows, ceiling lights, or other sources of radiation, black shields were installed on the opposite side of the strip (they are marked as "shield" in Fig. 4). The shields worked well but could not block all reflections. In particular, the area immediately under the pyrometer shows some reflections from the induction furnace. Also, the area above the

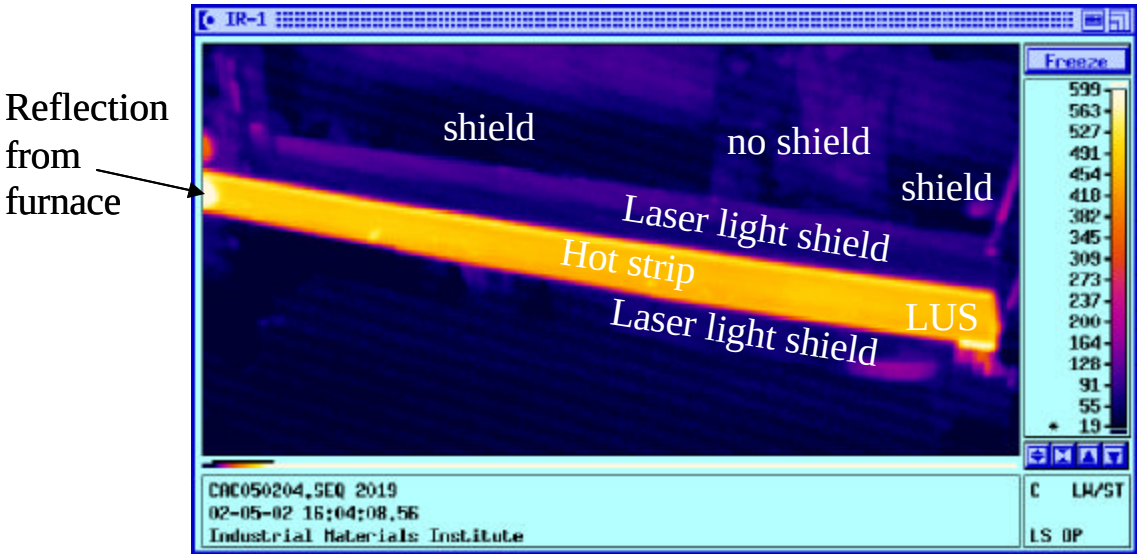


**Figure 4.** IR camera image of coil 5754-3 taken near the end of the temperature plateau shown in Fig. 1. The laser light shields prevent the escape of laser radiation from under the strip. The other shields block IR radiation from windows to the outside of the plant and from ceiling lights. The region indicated by "no shield" did not have IR shields. The pyrometer measured the temperature on the far left of the picture where a reflection of IR radiation from the furnace can be seen. The laser ultrasound measurement area was under the "S" of "LUS". The color scale on the right is for temperature in °C.

staircase to the walkway (a length of about 1 m along the strip) had no such shield. However, it is easy to identify those areas from the infrared image and to avoid using them in the analysis.

To calibrate the IR image into temperatures, the emissivity of the strip must be entered into the imaging software. This number was unknown to us. So instead, the emissivity was adjusted until the indicated temperature agreed with that which was evaluated using the pyrometer. For that purpose, we chose the stable conditions shown in Fig. 1 for Sample 5754-3 between 60 and 90 seconds. The emissivity so obtained was 0.104, which is a reasonable value. This value was then used to analyse all samples for the two days. It is well known that the emissivity of aluminum varies substantially and it is likely that our procedure produces large errors. This is especially true for the second day when a different alloy was used (5052) and no new calibration could be obtained because the pyrometer did not work.

Figure 5 shows the same image as Fig. 4, except that the temperature scale is magnified to show the range between 400 and 500 °C (752 to 932 °F). A number of hot spots are observed, as well as regions of warmer and cooler temperatures. Because the strip is slowly cooling when moving from left to right, we would expect a gradual change in temperature but this is not the case. Instead the apparent temperature varies within a range of about 40 °C (72 °F), as shown in Fig. 6, and a range of about 50 °C (90 °F) during the temperature plateau shown in Fig. 2. Because, in that region of the strip, the pyrometer values were relatively constant, the most likely explanation for the apparent temperature variation is fluctuations in surface emissivity.

Therefore, we believe that the pyrometer values are much more repeatable that the IR camera values. Unfortunately, because of the pyrometer breakdown on the second day, the only available temperature values for that day are the imprecise values of the IR camera.

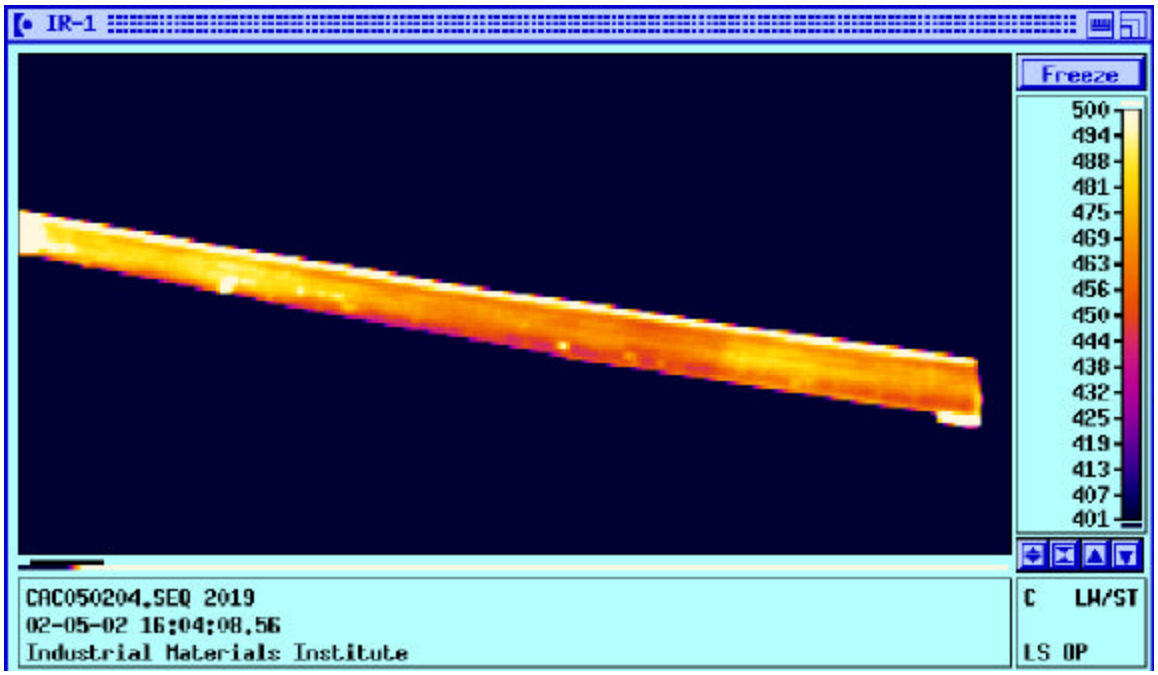


**Figure 5.** Same as in Fig. 4 except that the temperature scale is magnified from 400 to 500 °C (752 to 932 °F).

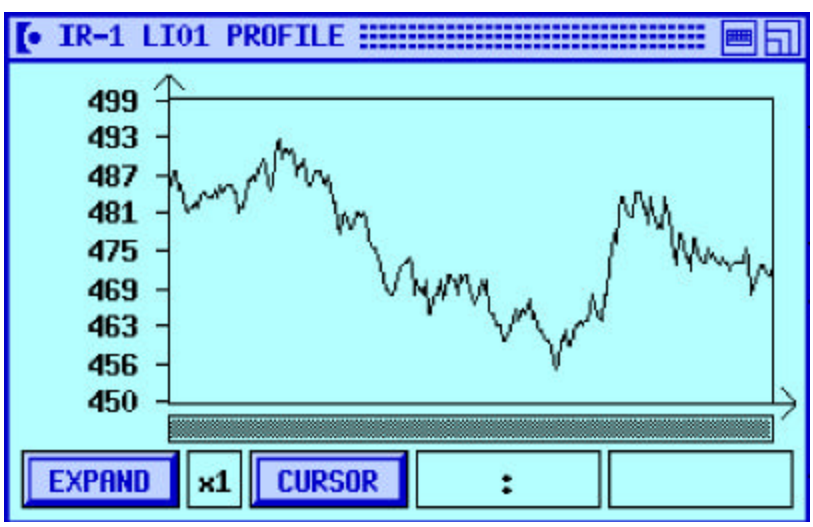


**Figure 6.** Temperature profile along a line following the center of strip shown in Fig. 5.

**Comparison of the Williamson pyrometer and the IR camera data**

To further verify the validity of the IR camera temperature readings, the IR camera temperature is plotted against the pyrometer values in Fig. 7. The solid line is a linear least squares fit of the data and shows that the two temperatures are linearly correlated as: T(IR Camera) = -40.4 + 1.130 * T(pyrometer). The slope is not one and the intercept is not zero to highly significant levels. Very likely, this is due to the estimate of the emissivity as explained above or to variations of emissivity with temperature. However, given that we believe the pyrometer values to be more accurate, this provides a means to correct for systematic errors in the IR camera temperature measurements. The root mean square (RMS) residual to the correlation is 18.1 °C (32.6 °F). The RMS residual is an estimate of the combined measurement error of the two pyrometers. Assuming that it is entirely due to the IR camera measurement, then we estimate that the IR camera measurement error is ±18 °C.

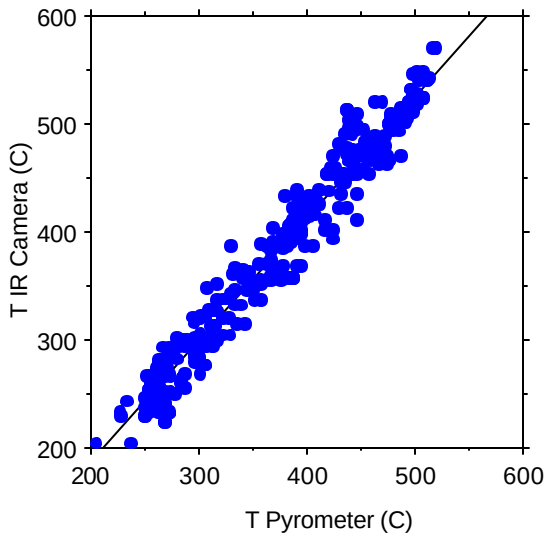


**Figure 7** IR camera temperatures vs. pyrometer temperatures.

**Temperature drop from the pyrometer to the laser-ultrasound measurement point**

The pyrometer was located near the exit of the induction furnace to best estimate the temperature rise induced by the furnace. On the other hand, the laser-ultrasound sensor was located as far from the furnace as possible to allow maximum time for recrystallization. The distance between the two was 12 feet. As the sheet moved from the furnace to the laser-ultrasound measurement location, its temperature dropped. The purpose of the IR camera was to measure that drop and provide a reliable estimate of temperature at the laser-ultrasound measurement location.

Figure 8 shows the temperature drop for samples 5052-1 through 5052-4 and a scrap 5052 coil. These coils had a gauge of 0.120 inches and the sheet speed on the mill was approximately

152 feet/min. As expected, the temperature drop increases with temperature. However, the linear relationship does not extrapolate to zero temperature drop when the furnace temperature is room temperature. The same is true for other combinations of gauges and mill speeds (see Fig. 9).

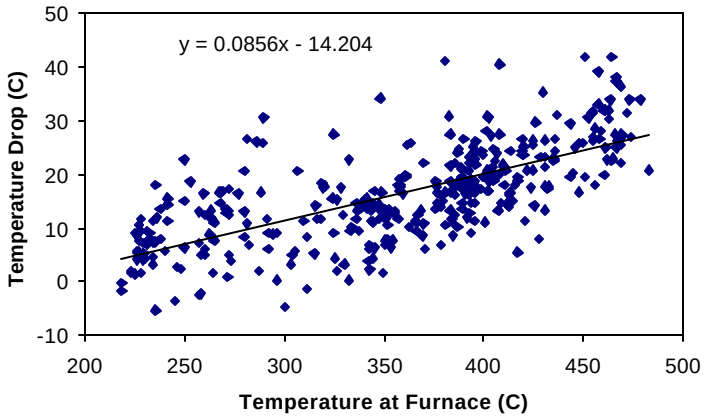


**Figure 8** Temperature drop between the pyrometer and the laser-ultrasound measurement point as estimated using the IR camera.

There are several possible explanations for this: The roller table is heated by the sheet and re-radiate this heat onto the bottom surface of the sheet; the emissivity of aluminum varies with viewing angle and the small angular difference between the two locations may cause some systematic error; the temperature drop vs. furnace temperature relationship may not be linear given that the motion of the sheet involves convective as well as radiative heat losses. These possible explanations were not investigated. The estimated temperature drop is thus a first order correction on the pyrometer reading. If a more accurate estimate were required in future measurements, the simplest and most reliable solution would be to use a second pyrometer.

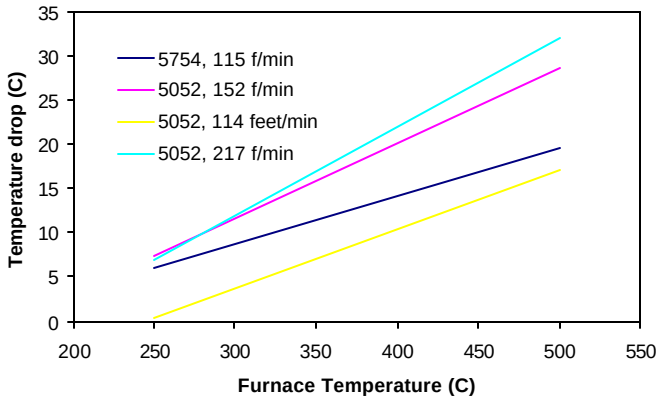


**Figure 9** Temperature drop between the pyrometer and the laser-ultrasound measurement point as estimated using the IR camera: Summary of results for four different sets of coils (only the linear least squares fits are shown).

It is also interesting to note from Fig. 9 that the faster the mill speed and the thinner the sheet, the larger the temperature drop, even though there is less time for the sheet to cool. This is because of the reduced gauge and because higher mill speeds increase convective cooling.

## *III Laser-ultrasonic measurements and discussion*

### Laser-ultrasound resonance spectroscopy, texture, and recrystallization

The basic principles of the prototype system are detailed in past documents[1] and prior publications.[2] In summary, an excimer laser sends a 15 ns, 600 mJ, pulse of ultraviolet (UV) light onto the strip surface. This high-energy pulse ablates a thin layer on the surface and launches an ultrasonic pulse in the thickness of the strip. The pulse is reflected back and forth between the two surfaces and sets up one longitudinal and two shear ultrasonic resonances together with their harmonics. When these pulses are reflected at the strip surface, they cause a small amount of surface motion. This motion is sensed by laser interferometry using another pulsed laser (200 $m$s duration, 200 mJ/pulse, infrared radiation) and a confocal Fabry-Perot interferometer. This technique is called Laser-ultrasound resonance spectroscopy (LURS). In the setup used at CAC, the repetition rate of the lasers is 40 Hz and the signals are averaged 20 to 100 times to improve signal to noise ratio. Therefore, the measurement rate is of order one per second.

The surface displacement is recorded as a function of time and analyzed to extract the various resonance frequencies. The ratio $k$ of longitudinal to shear fundamental resonance frequencies is computed to provide an ultrasonic measurement that is independent of thickness. This ratio depends on crystallographic texture and on temperature (which is measured independently, as discussed in the previous section). As the aluminum strip recrystallizes, its texture changes in a manner that is characteristic of the alloy and of prior processing. The measured fractional change in texture (and therefore $k$ ) is used to estimate the recrystallized fraction.

### Laser-ultrasound prototype description

A picture of the prototype system is shown in Fig. 10. To the left, there are two belts that were used to guide the strip through the furnace. The Williamson pyrometer was located at the end of the belts and approximately 2 feet above the line. The strip (not shown) moved to the right onto the roller table and continued onto a coiler located some distance to the right edge of the image. A “push-down” roll was located near the right end of the roller table. Once the sheet was securely attached to the coiler, the roll came down and to the right, and kept the strip at a relatively constant height above the roller table. The laser-ultrasound sensor was the large blue box located below the roller table. Below the push-down roll on the image, a hole can be seen in roller table. This hole allowed the laser light to go from the laser-ultrasonic sensor to the strip and back to the sensor.

The blue box contained the excimer laser used to generate the ultrasound. The laser interferometer and related computers and electronics were remotely located in a small wooden cabin (not shown). The light was transported between the laser interferometer and the roller table using optical fibers. The laser interferometer light propagated in air between the end of the fibers and the strip, through the hole in the roller table.

The picture also shows aluminum shields installed on the edges of the roller table to block the laser light that could escape from underneath the strip. Laser safety and other safety hazards

were studied in details and are documented in a separate Safety Assessment report.[3] Laser light levels were measured inline, in simulated operating conditions (i.e. with a strip above the hole) before the experiments began. They indicated that safe levels were attained beyond a few feet of the roller table hole. Nevertheless, a safety perimeter was enforced. In this perimeter, laser safety goggles were mandatory in case of malfunction of any one of the components (furnace, laser sensor, strip guiding) of this experimental setup.

**Figure 10.** Picture of the laser-ultrasound sensor (large blue box) located under the roller table. The laser light travels between the sensor and the aluminum sheet through a small hole in the roller table. The hole is located immediately to the right of the sensor.

## Description of data analysis

In this section, the signal processing and analysis to obtain the longitudinal and shear resonance are described. A typical waveform showing multiple echoes in the sheet thickness is shown in Fig. 11.

In laser-ultrasound resonance spectroscopy, the Fourier transform of the recorded time signal is performed to distinguish the natural resonances in the thickness of the sheet. A Blackman-Harris window is used to reduce spectral leakage and enhance the detectability of the low-amplitude shear resonances. For the temperature range of interest, the signal to noise ratio of the shear wave for single shot experiments is not always sufficient to distinguish shear resonances. Therefore, it is often necessary to average the signal to increase the signal to noise ratio. However, as we will show later in this report, the aluminum sheet thickness varies relatively rapidly and by several percents. These thickness variations shift the resonance frequencies and, as a result, a simple signal averaging procedure would broaden the peaks and would not improve the signal to noise ratio much.
To correct for thickness variations, it is assumed that the wave velocities do not change during the averaging. This is equivalent to assuming that texture variations are small while we average the signal. Using this assumption, thickness variations cause variations in the resonance frequencies. This is equivalent to a dilatation (or compression) of the frequency axis. An equal

and opposite dilatation is applied numerically and the resulting spectrum is then interpolated using a spline function to match a preset frequency scale. The obtained complex spectra are then summed together. Depending on temperature and thickness, between 20 and 100 traces are averaged. In Fig. 11, a time signal is presented. Figures 12 to 14 present amplitude spectra, without averaging (Fig. 12), with averaging of 100 shots with thickness variations correction (Fig. 13) and without thickness variations correction (Fig. 14). Clearly, it is necessary to apply thickness variation corrections to distinguish the shear wave resonances with amplitudes near –60 dB. The sixth harmonic shear resonance and the fourth harmonic longitudinal resonance locations are indicated with blue and red lines, respectively.

If all harmonics of the fundamental longitudinal resonance are easily identified in the signal spectrum, this is not true for the harmonics of the fundamental shear resonance for which only some harmonics exceed the noise level. At too high a temperature, the identification of the shear resonance is no more possible due to high wave attenuation. Therefore, much effort has been directed to identifying and measuring shear resonances with small signal to noise ratio.

As a result, while the measured fundamental longitudinal frequency is the average of all harmonics up to a maximum frequency, the measured shear fundamental frequency is given by a few selected harmonics that are more easily identified. It was found that the sixth harmonic is often the easiest one to measure. However, all shear harmonics exceeding the noise level are measured and averaged.

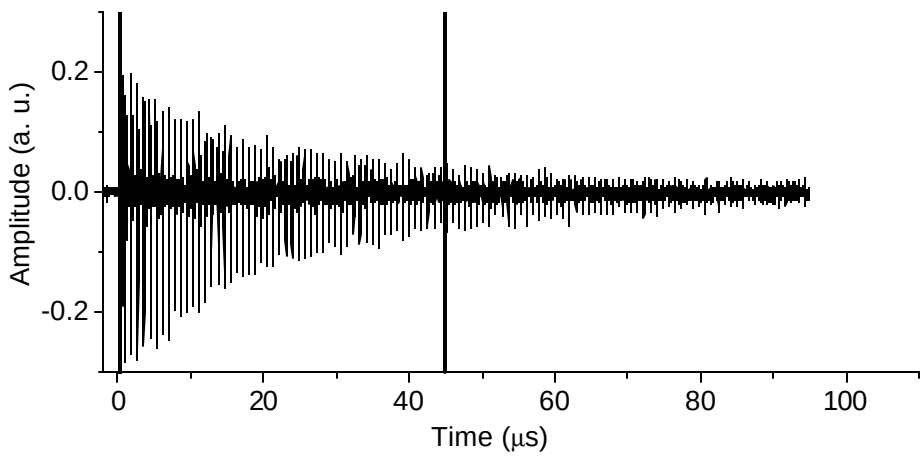


**Figure 11.** Time signal.

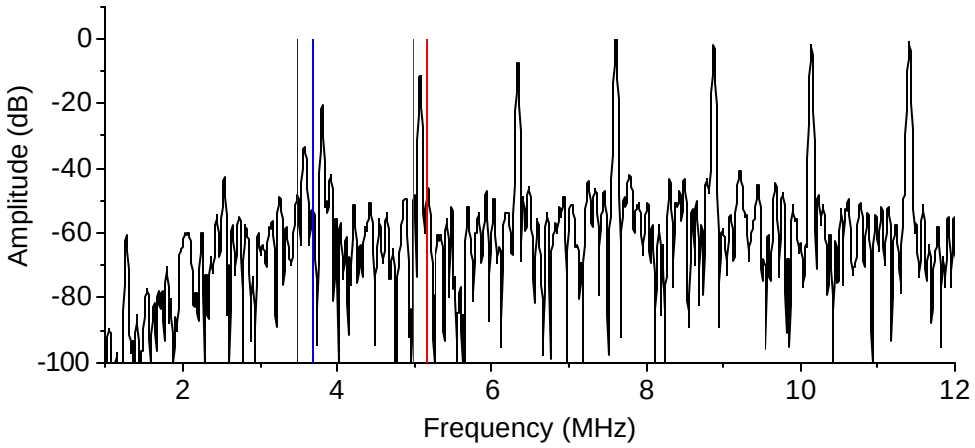


**Figure 12.** Amplitude spectrum for single shot experiment.

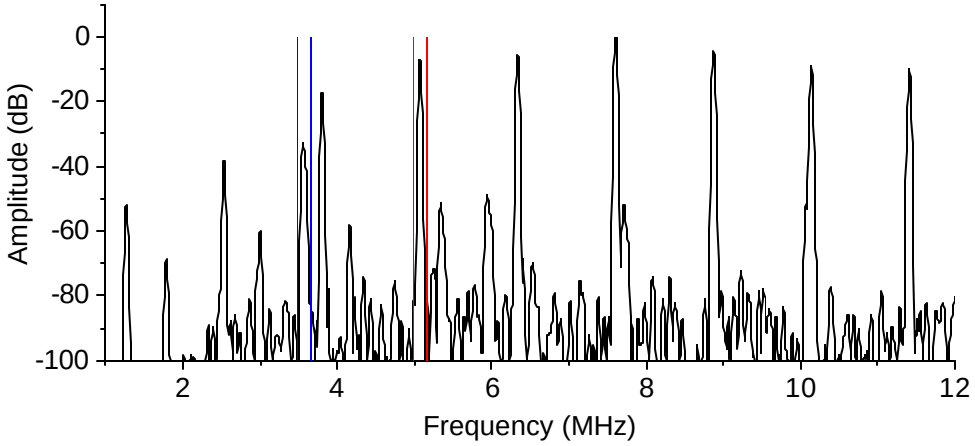


**Figure 13.** Amplitude spectrum for 100 shots averaging with thickness variation correction.

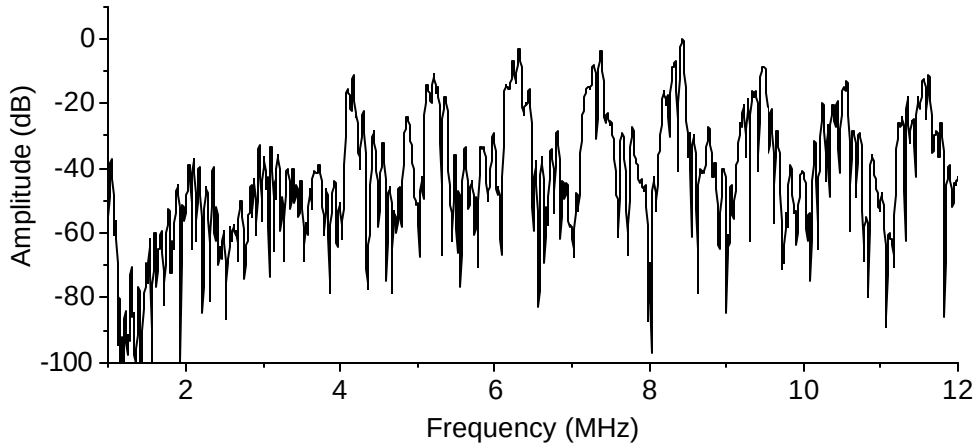


**Figure 14.** Amplitude spectrum for 100 shots averaging without thickness variation correction.

## Inline laser-ultrasonic measurements

*Measurement procedure*

The online measurements were made on short trial coils with lengths ranging from 100 to 1000 feet. At the beginning of each coil, the induction furnace was off and the relatively high temperature of the strip was entirely due to prior processing (twin belt casting and hot rolling). The laser-ultrasonic measurements began shortly after the front end of the coil had arrived and continued up to a few meters from the end of the coil. As the coil was made, the induction furnace power was ramped up manually in steps. The clocks of the laser-ultrasonic and temperature measurements systems were synchronized and all the natural representation of the raw data is as a function of time (which is proportional to length) along the strip.

*Temperature measurements*

As described in Section I on Pyrometry, this report utilizes the temperature measurements obtained with the IR camera. The camera provides a complete temperature profile along the roller table. However, two locations are of higher interest. First, the temperature near the exit of the furnace is very important because it indicates the furnace temperature required to obtain recrystallization. Second the temperature at the LURS measurement location (or LUS for Laser-ultrasound) is essential to remove temperature effects from the ultrasonic data. In the Figures to be presented in this report, the two temperatures are referred to as “Furnace temperature” and “LUS temperature”, respectively.

The camera was operating continuously, taking one image of the entire strip between the furnace and the LURS measurement location every two seconds. The clock of the camera was synchronized with the LURS computer clock so that the two measurements could be matched later, during the data analysis.

*Longitudinal resonances and thickness:*

The variations of the longitudinal fundamental frequency measured for coil 5754-2 is presented in Fig. 15 without averaging. The computer used for the LURS measurement provides the time basis. The sheet temperature shown in this graph is that provided by the IR camera at the LURS measurement location. The longitudinal fundamental frequency $f_L$ depends on thickness and longitudinal velocity as

$$f_L = \frac{v_L}{2e}, \qquad (1)$$

where $v_L$ is longitudinal velocity and *e* is sheet thickness. The longitudinal fundamental frequency oscillations are most likely due to thickness variations of about 4%.

In general, when texture does not change, the elastic constants of aluminum are expected to decrease as temperature increases. This is also illustrated in Fig. 15. This decrease in resonance frequency with increasing temperature was observed for all coils except for the last four coils of the second measurement day. Figure 16 shows variations of the longitudinal fundamental frequency as a function of time for coils 5052-11, 5052-12 and 5052-13. A signal averaging of 20 is used to reduce the amplitude of the oscillations. An increase of 50% in the longitudinal fundamental frequency is observed. In Figure 17, this same variation in longitudinal

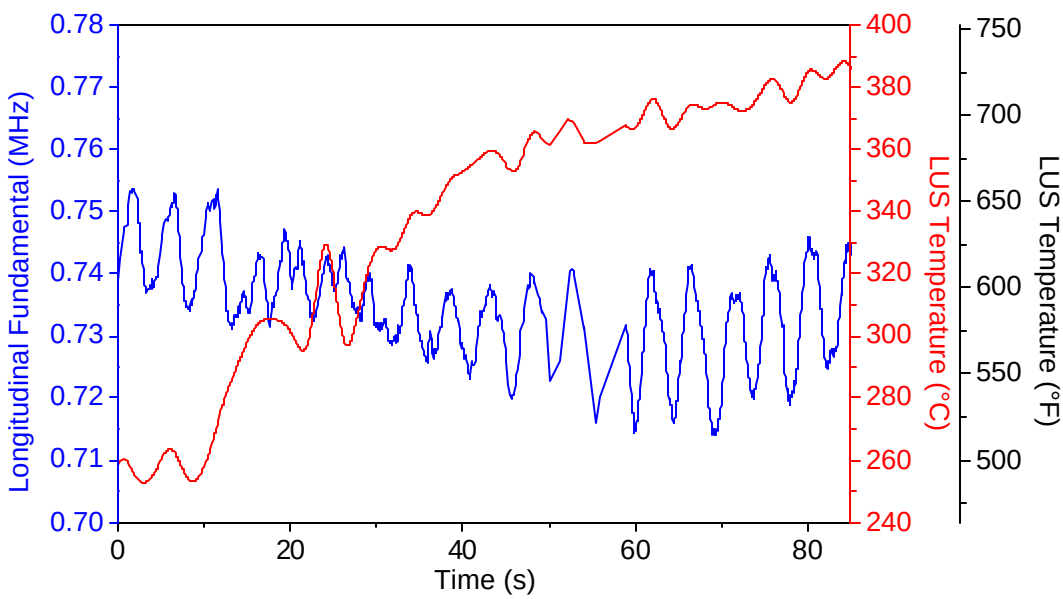


**Figure 15.** Longitudinal fundamental frequency and temperature as a function of time for coil 5754-2.

fundamental frequency is presented for coil 5052-13 together with the measured temperature at the LUS measurement location. For this coil, the longitudinal velocity increases with increasing temperature. Similar results were observed for coils 5052-10, 5052-11 and 5052-12. These large increases in longitudinal resonance frequency are probably caused by a long-term drift in strip thickness. This explanation is supported by thickness measurements made on three samples for the coil 5052-11. Two samples taken after the induction furnace near the end of the coil have thicknesses of 2.17 and 2.28 mm, while one sample taken before the induction furnace near the beginning of the strip has a thickness of 2.78 mm. This 25% decrease in thickness is comparable to the increase in resonance frequency of 20 % observed in Figure 16 for the same coil.

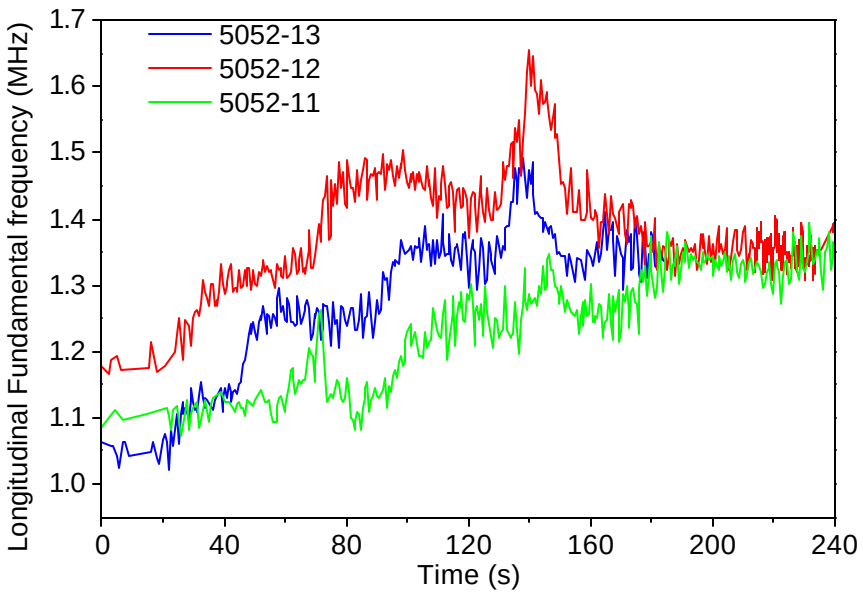


**Figure 16.** Longitudinal fundamental frequency as a function of time for coils 5052-11, 5052-12, and 5052-13.

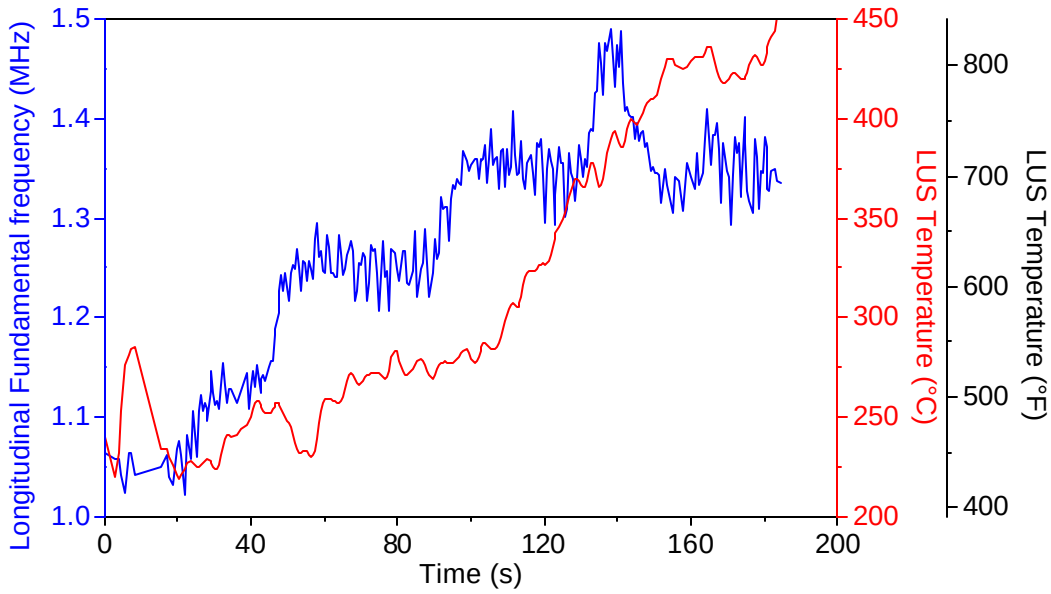


**Figure 17.** Longitudinal fundamental frequency and temperature as a function of time for coil 5052-13.

Because the longitudinal (and shear) resonance frequency depends on thickness, it cannot be used alone to provide information on recrystallization. Instead, we use the ratio of longitudinal and shear resonance frequencies because this ratio is insensitive to thickness.

*Ratio of resonance frequencies*

The ratio of longitudinal to shear fundamental resonance frequencies, $k$ , provides an ultrasonic measurement that is independent of thickness. However, this ratio depends on the temperature-dependent, single-crystal elastic constants and depends also on crystallographic texture. More specifically, an increase in temperature tends to increase $k$ while recrystallization tends to decrease $k$ .

Figure 18 presents the $k$ ratio and temperature measured as a function of time for the first coil of the first day. This coil (and a few others) is referred to as “Calibration”. No recrystallization signature can be observed in the evolution of the $k$ ratio because $k$ increases monotonically with temperature.

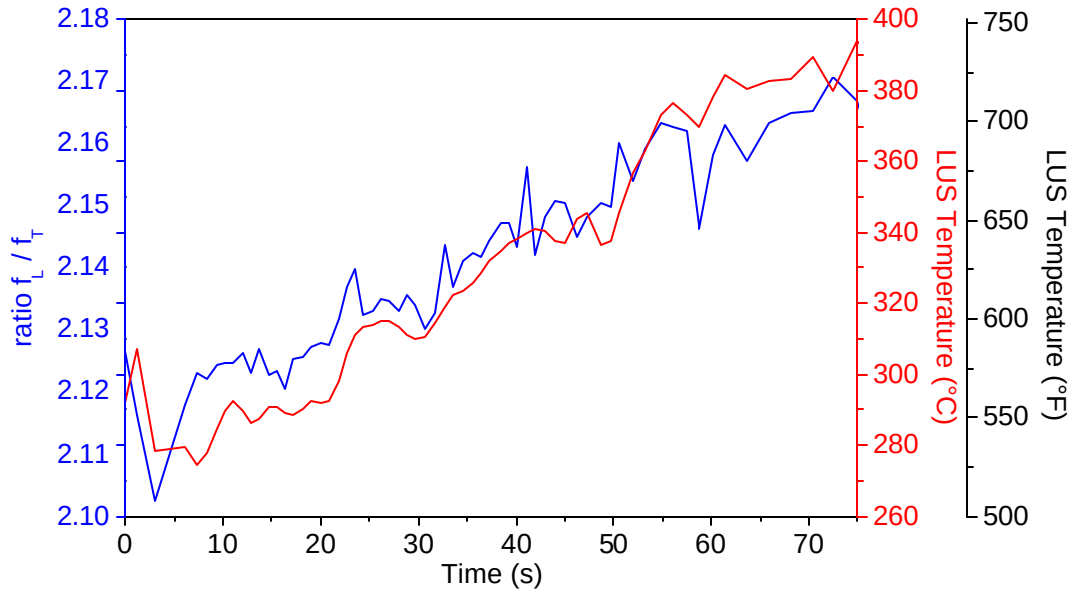


**Figure 18.** $k$ ratio and temperature as a function of time for the first coil of the first day (referred to as "Calibration", grade 5754).

In Figure 19, the $k$ ratio for coil 5754-2 drops while temperature increases. This is interpreted as a texture change caused by recrystallization. The recrystallization seems to begin at the time 40 s and at a temperature of 360 °C (680 °F, measured at the LUS measurement location). At this time, $k$ begins to decrease slowly to reach a sudden minimum at a time near 80 s and a temperature of 380 °C (716 °F). After the minimum, $k$ increases again, presumably because of the increase in temperature. The total decrease in $k$ is approximately 0.02.

In Figure 20, the $k$ ratio for coil 5754-4 hints that recrystallization may occur at the time 35 s and at a temperature of 370 °C (698 °F, measured at the LUS measurement location). The observed decrease in $k$ would be approximately 0.01. This signature is barely larger than the measurement noise observed between 20 and 30 seconds. Although this drop is barely significant by itself, it is somewhat credible because it happens at the same temperature as for coil 5754-2 of Figure 19.

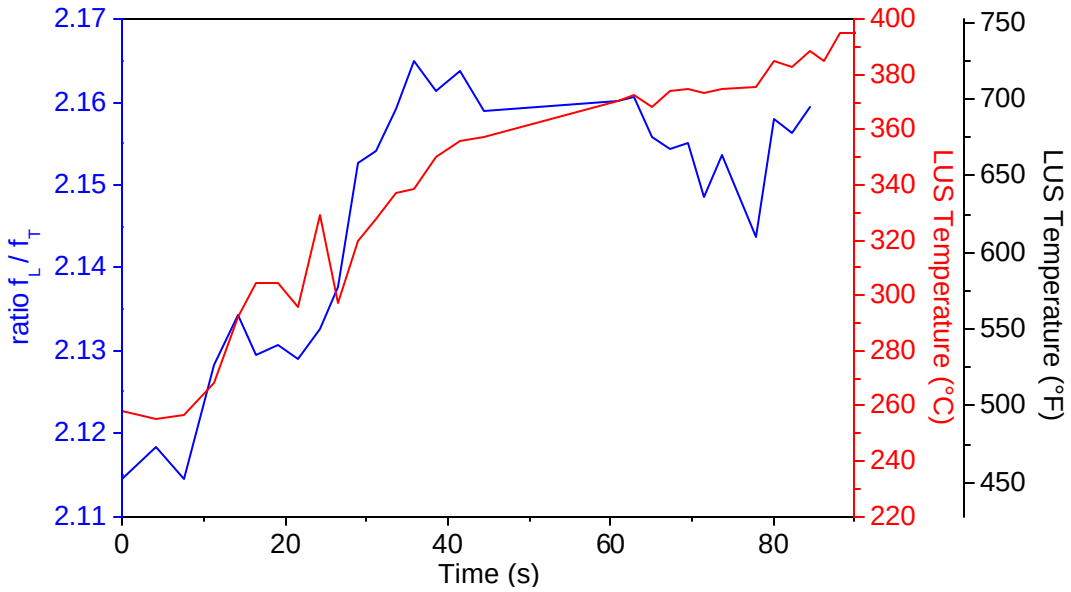


**Figure 19.** *k* ratio and temperature as a function of time for coil 5754-2.

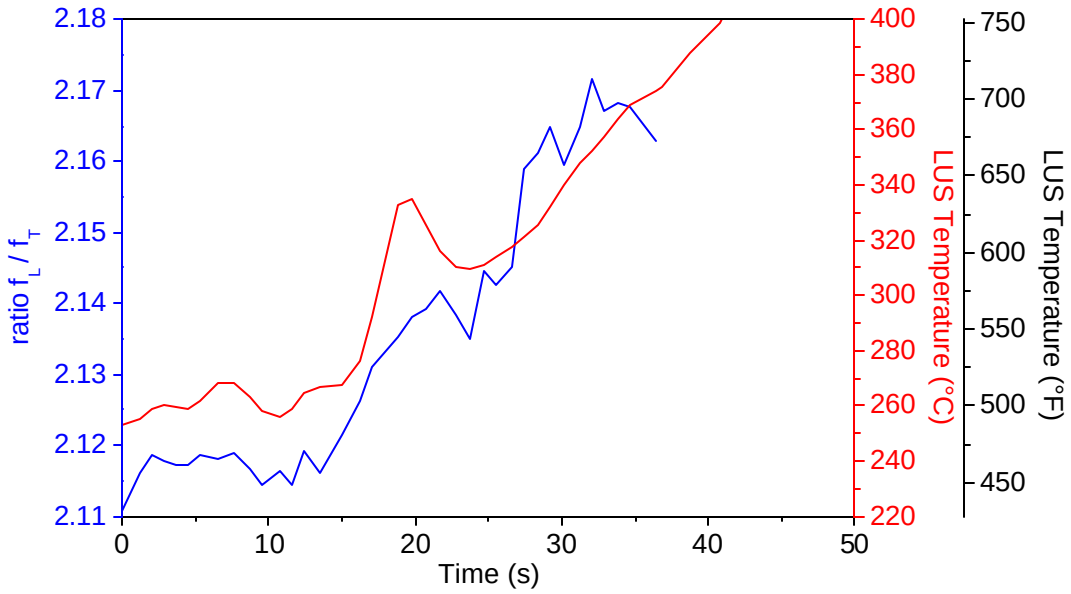


**Figure 20.** *k* ratio and temperature as a function of time for coil 5754-4.

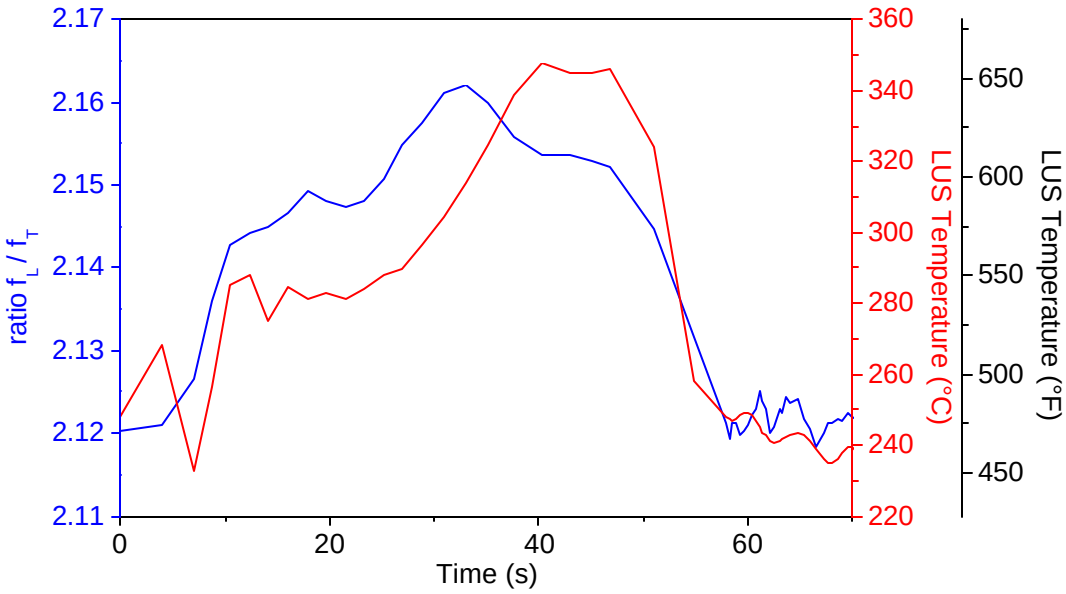


**Figure 21.** $k$ ratio and temperature versus time for the last coil of first day (referred to as "scrap", alloy 5754).

For the last coil of the first day (referred to as "scrap", alloy 5754), the $k$ ratio drops as temperature increases above 320 °C (608 °F) at the LUS measurement location (Figure 21). The $k$ ratio reaches its lowest value at a temperature of about 340 °C (644 °F), but this may not be the temperature of minimum $k$ ratio as the temperature was not allowed to go any higher. The observed decrease in $k$ was approximately 0.01.

The $k$ ratio versus time for coils 5052-12 and 5052-13, shown in Figure 22 and 23, also displays a recrystallization signature. Near 325 °C (617 °F, at the LUS measurement location) the $k$ ratio drops while the sheet temperature increases. The observed decrease in $k$ is approximately 0.01. Note that, after the recrystallization signature, no data for the $k$ ratio can be measured since the low signal to noise ratio of the shear waves is not sufficient to distinguish shear resonances.

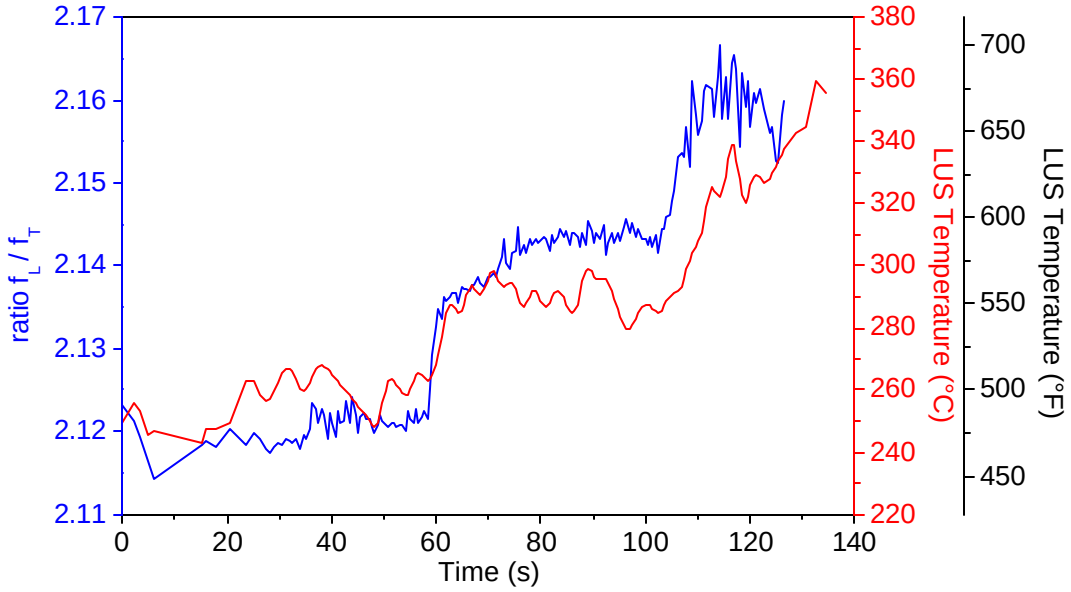


**Figure 22.** *k* ratio and temperature versus time for coil 5052-12.

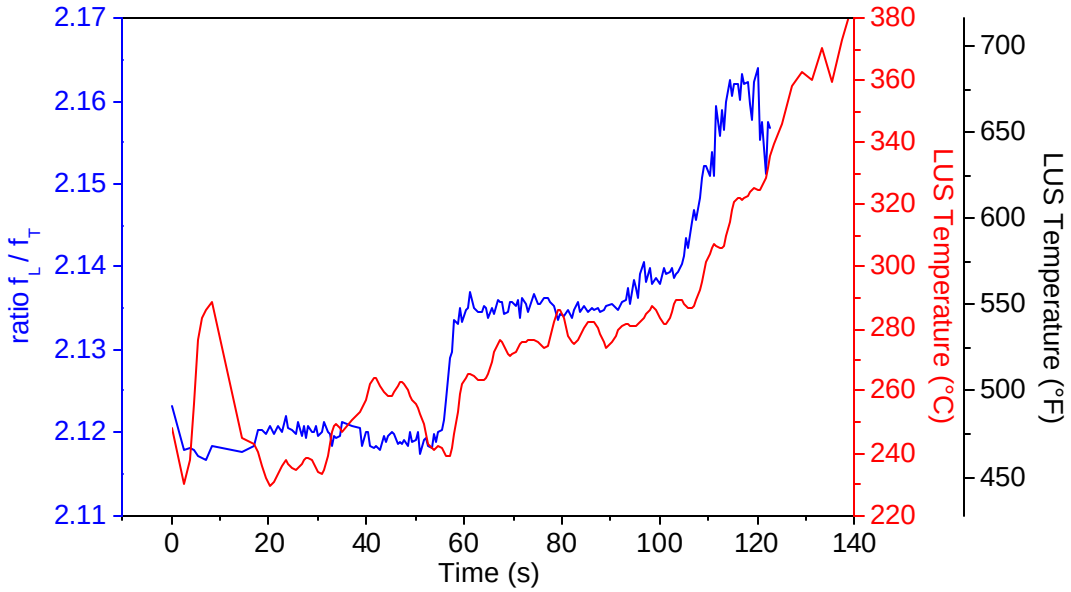


**Figure 23.** *k* ratio and temperature versus time for coil 5052-13.

The recrystallization signature may also be shown in a different representation: the $k$ ratio versus temperature. With increasing temperature, the $k$ ratio should increase almost linearly with temperature when no texture change occurs while it should decrease linearly with texture changes caused by recrystallization, as previously reported by C.-S. Man et al.[4] and Kruger et al.[5]

In Figure 24, the $k$ ratio for coil 5754-2 increases linearly with temperature up to 360 °C (680 °F) but decreases significantly above 360 °C. Note that, in contrast with Figures 15 to 23, the temperature reported on Figure 24 (and Figures 25 to 29) is that measured with the IR camera near the exit of the furnace. The observed drop in $k$ was approximately 0.01 to 0.02 depending on whether the apparent drop near 380 °C (716 °F) followed by an increase near 400 °C (752 °F) is interpreted as the end of recrystallization followed by a return to a linear increase of $k$ with temperature or interpreted as measurement error.

In Figure 25, for the coil ID 5754-4, the $k$ ratio increases linearly with temperature up to 360 °C (680 °F) and drops at higher temperatures. Again, this is interpreted as a signature of recrystallization. The observed drop in $k$ is approximately 0.01. A larger drop might have been observed if the shear signal had not been lost at higher temperatures.

In Figures 26 and 27, for the coils 5052-12 and 5052-13, the $k$ ratio also presents a recrystallization signature near 340 °C (644 °F).

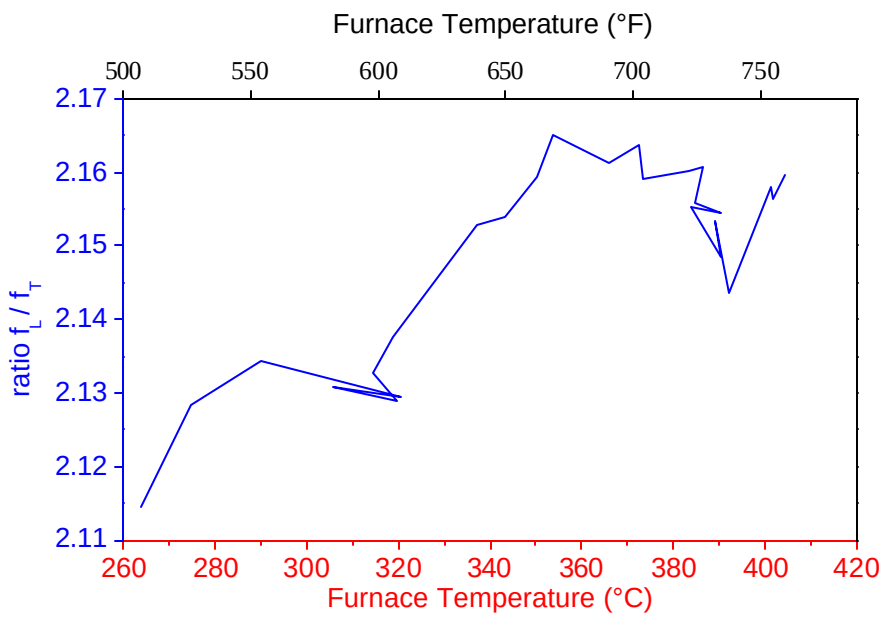


**Figure 24.** $k$ ratio versus temperature for coil 5754-2.

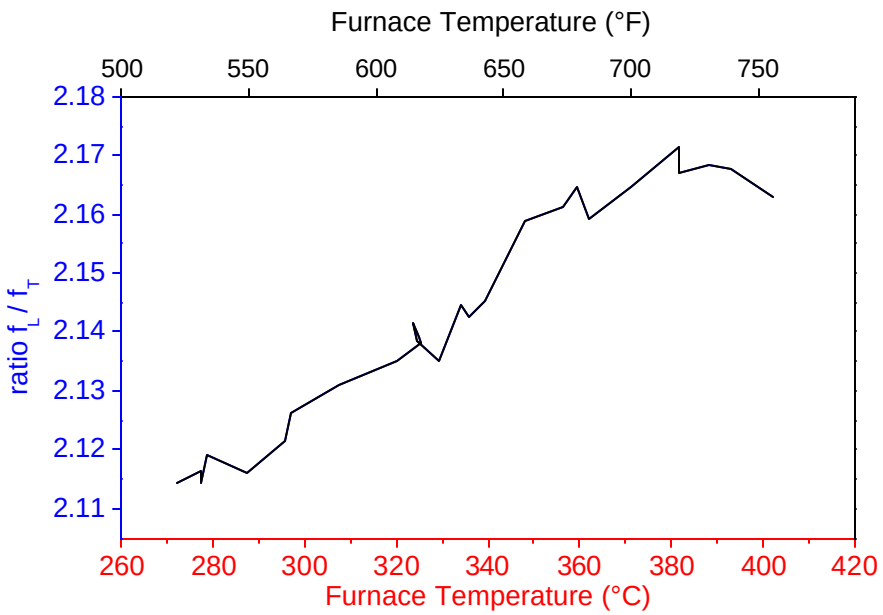


**Figure 25.** *k* ratio versus temperature for coil 5754-4.

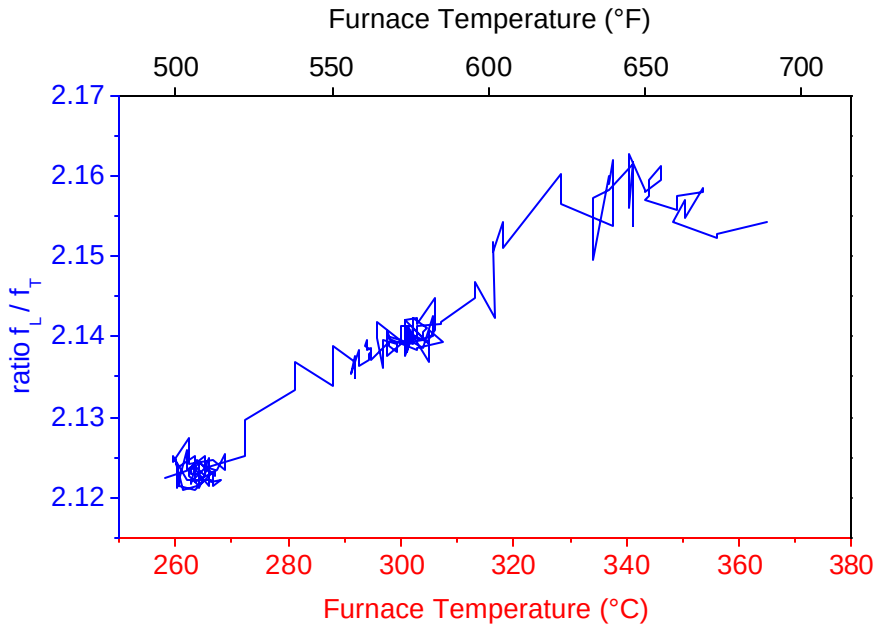


**Figure 26.** *k* ratio versus temperature for coil 5052-12.

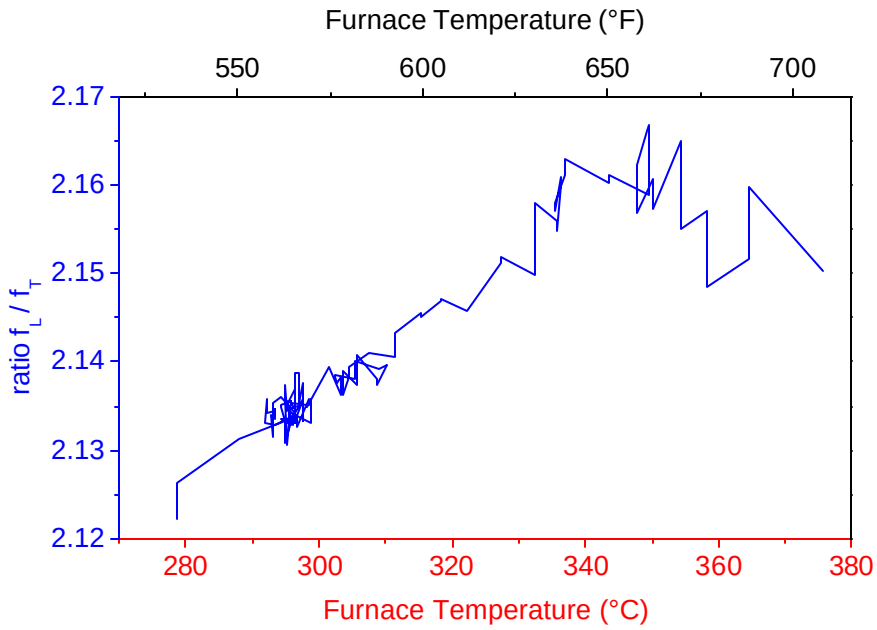


**Figure 27.** $k$ ratio versus temperature for coil 5052-13.

Figures 28 and 29 summarize the results of Figures 24 to 27 for the two grades 5754 and 5052. Figure 29 also includes additional results for coils 5052-11and 5052-6. It can be observed that the temperature dependence of the $k$ ratio is the same (to within experimental error) for all coils of a given grade. The ratio increases with temperature up to a maximum temperature. Above this temperature, $k$ decreases slightly and this is interpreted as a signature of recrystallization. From these two Figures, we estimate that alloy 5754 begins to recrystallize near 380 °C (716 °F) and alloy 5052 begins to recrystallize near 350 °C

In conclusion, Figures 19 through 29 show that the ratio of longitudinal to shear fundamental frequencies, $k$, as measured inline at CAC, displays the expected signature for recrystallization. Moreover, the magnitude of the observed decrease (at least 0.01 in five cases and approximately 0.02 in one case) is close to the observed decrease of approximately 0.02 observed in the laboratory by C.-S. Man et al. Therefore, we conclude that recrystallization can be measured inline using laser-ultrasonic resonance spectroscopy.

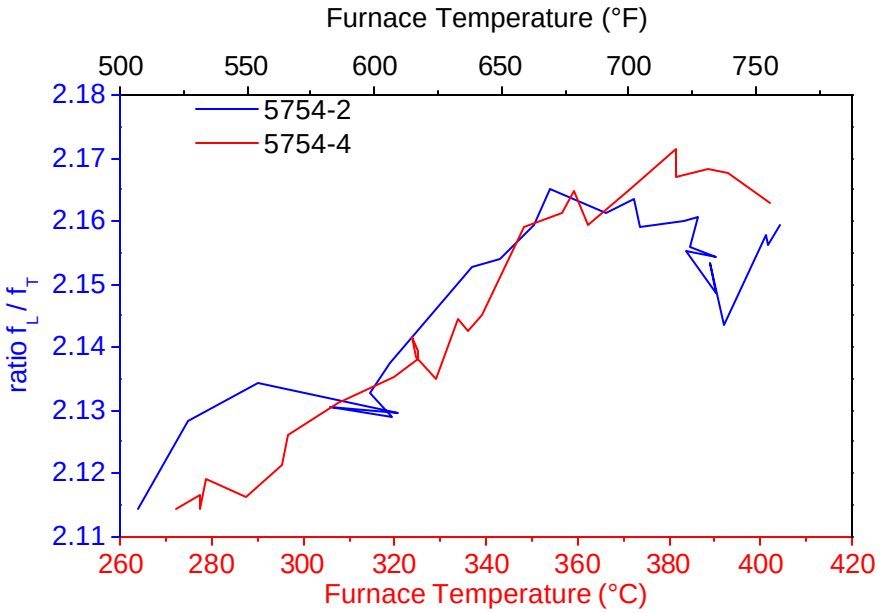


**Figure 28.** *k* ratio versus temperature for coils 5754-2 and 5754-4.

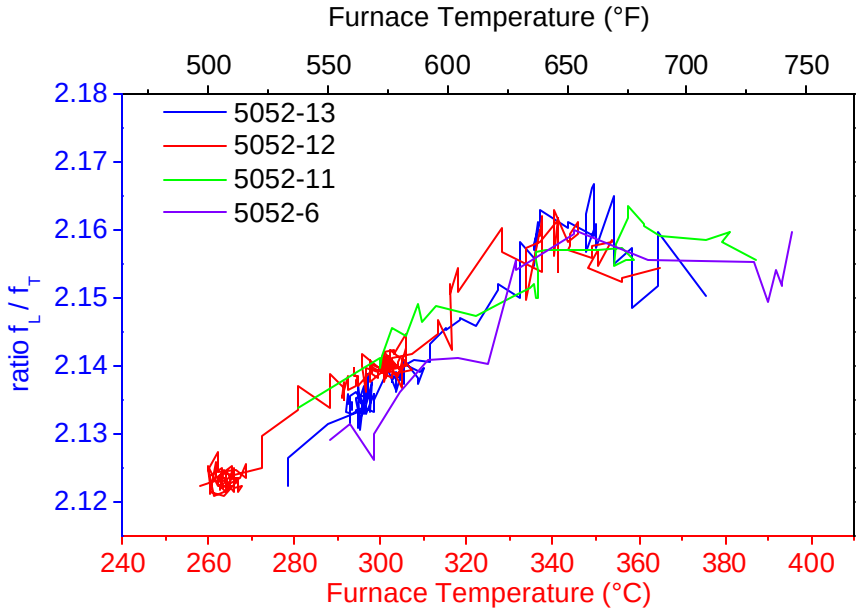


**Figure 29.** *k* ratio versus temperature for coils 5052-11, 5052-12, 5052-13, and 5052-6.

**Measurement limit, validity and accuracy**

As previously described, the recrystallization of aluminium coils has been measured inline. The $k$ ratio versus temperature gives a clear signature of recrystallization. The inline results are limited by the poor signal to noise ratio of shear waves at high temperatures. The shear resonances disappear rapidly with increasing temperature and, for some coils, no recrystallization signature can be observed.

The $k$ ratio was measured up to inline temperature of 400 °C (750 °F) at the exit of the furnace (380 °C at the LUS measurement point) for grade 5754 and up to 380 °C (360 °C at the LUS measurement point) for grade 5052. The $k$ ratio is measured when the signal to noise ratio of the shear resonance exceeds 2 dB. In contrast, the longitudinal fundamental frequency was measured for laser-ultrasound temperatures up to 460 °C (860 °F).

Figure 30 shows the $k$ ratio, the temperature and the attenuation of the longitudinal waves for coil 5052-13. For this coil, the $k$ ratio was measured up to the time 120 s corresponding to a LUS temperature of 380 °C (716 °F). For higher temperatures, the shear resonances disappear. For this coil, the $k$ ratio was obtained up to and during recrystallization but not after. As a result, the onset of recrystallization is detected inline but we cannot conclude on the recrystallization state of the strip (percentage of recrystallization) for which the $k$ ratio at higher temperatures is necessary. In Figure 30, the attenuation of the longitudinal waves was evaluated by narrow-band filtering the time signal around the longitudinal resonance frequency closest to 12 MHz (attenuation depends on frequency so a fixed frequency must be chosen) and by calculating the envelope of this filtered signal. The envelope is given by the complex modulus of the Hilbert transform. An exponential fit of the envelope gives the attenuation of the longitudinal waves near 12 MHz. The attenuation, or exponential decay of the signal, is expressed in Nepers per $m$ s (1 Np = 1/*e* = 0.3679).

Several factors explain why the shear resonances are not observed at temperatures as high as for longitudinal resonances. Figure 30 shows that the attenuation increases rapidly with temperature above 400 °C (752 °F) for the longitudinal waves. With the signals collected at CAC, we cannot evaluate the attenuations of shear waves. Previous work at IMI on AA5754 has shown that the rapid increase of attenuation with temperature begins at a lower temperature for shear waves than for longitudinal waves (Figure 31). From this work, we estimate that the longitudinal wave attenuation is comparable to the shear wave attenuation at a temperature that is 75 °C (135 °F) lower. A second reason for the lower signal to noise ratio of the shear resonances is that the longitudinal waves are generated and detected more efficiently than the shear waves. There are some possibilities to improve the sensitivity of the apparatus to shear resonances, including improved optical configuration of the laser beams and increased signal averaging. Because of the rapid increase in attenuation with temperature, a large increase in sensitivity would only provide a relatively small increase in temperature. In fact, Figure 31 may be used to estimate that near 425 °C (800 °F), the attenuation increases by a factor of two for a temperature increase of 40 °C (72 °F). Therefore, to increase the maximum temperature by 40 °C, we would need to increase the signal to noise ratio by some amount that is difficult to estimate but that would be at least 6 dB. However, because recrystallization is a thermally activated process and because recrystallization of AA5754 happens approximately ten times

faster for each 25 °C (45 °F) increase, we do not expect that the sensor would be required to operate at temperatures much higher than those employed during these tests. In summary, the inline recrystallization measurement is limited in temperature by the detectability of shear resonances.

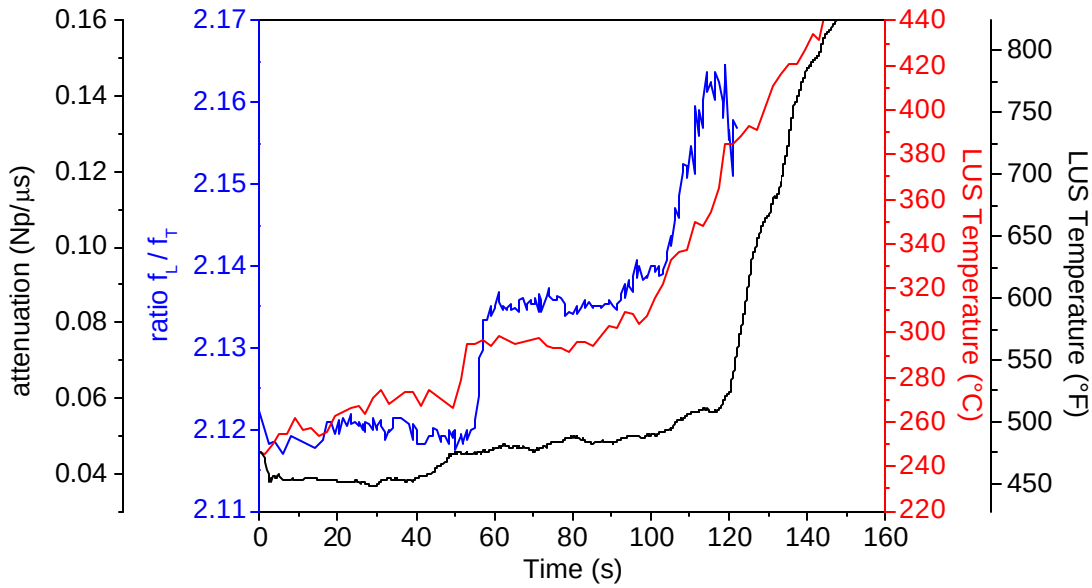


**Figure 30.** $k$ ratio, LUS temperature and attenuation of longitudinal waves near 12 MHz versus time for coil 5052-13, as measured inline.

The measurement accuracy of the $k$ ratio is difficult to assess because $k$ varies with temperature and the temperature data are not precise. The repeatability of the $k$ ratio measurement is estimated by considering a series of measurements where the temperature is expected to be relatively constant and where no texture change occurs. For the coil 5052-13, there is a temperature plateau between 60 and 90 s when the induction furnace heating power was most likely constant (Figure 30). During this plateau, the standard deviation of the $k$ ratio is ± 0.0008, or less than ± 0.04 % of the mean value. For higher temperatures, when the shear resonance signal to noise ratio is lower, the accuracy decreases. The $k$ ratio has the strongest fluctuations between 115 and 120 s. The standard deviation of these fluctuations is less than 0.1 %. From this, we can estimate that the upper limit to the precision of the $k$ is of order of 0.1 % for temperatures of about 360 °C (680 °F).

In ending this discussion on measurement error and validity, we would like to comment that much better experimental results would have been achieved if the temperature had been ramped up slowly and if longer coils had been made. For many samples, the temperature went above recrystallization before we could accumulate enough data. Conversely, the three longest coils (5052-11,12,13) gave the best results. Consequently, we are confident that future tests (if any) will provide even better results.

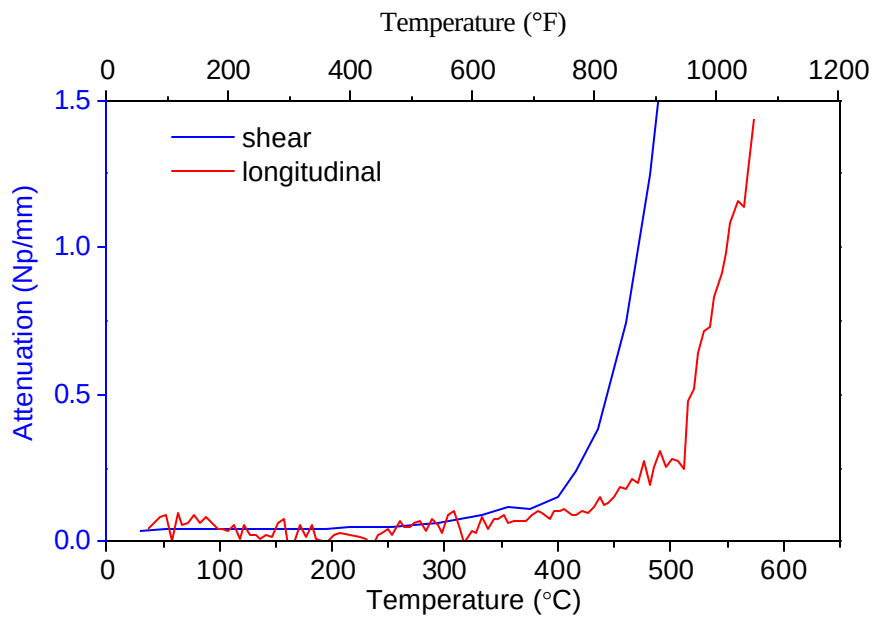


**Figure 31.** Attenuation of shear and longitudinal waves near 20 MHz versus temperature measured in laboratory for a 5754-aluminum grade.

### Supporting laser-ultrasonic measurements in the laboratory

To further validate the inline measurements, additional measurements were made in the laboratory using a Gleeble thermomechanical simulator coupled to a laser ultrasonic system. Two samples were selected from each of the two grades: a hot band sample (ID 5754-6 HB and ID 5052-11 HB) and an inline annealed sample (ID 5754-6, 850 °F and ID 5052-11, 700 °F). The samples were heated in the Gleeble to 500 °C (932 °F) and cooled back to room temperatures. The heating and cooling rates were 1 °C/s. Figures 32 and 33 show the $k$ ratio measured in situ during thermal processing.

Metallographic and texture measurements of the inline annealed samples show that these samples were fully recrystallized before they were heat treated in the Gleeble. In agreement with this, the two annealed samples displayed a completely reversible behaviour of $k$ vs. temperature. On the other hand, the hot bands samples are not expected to be recrystallized and recrystallization should occur during thermal treatment in the Gleeble. This is observed as a sharp drop in $k$ vs. temperature in Figures 32 and 33. Once fully recrystallized, as the temperature is raised to a maximum value and subsequently lowered back to room temperature, the dependence of $k$ on temperature for the hot band samples is identical to that of the inline annealed samples. It is interesting to note that the temperature of the beginning of recrystallization is approximately 370 °C (700 °F) for the alloy 5754, and approximately 390 °C (730 °F) for the alloy 5052.

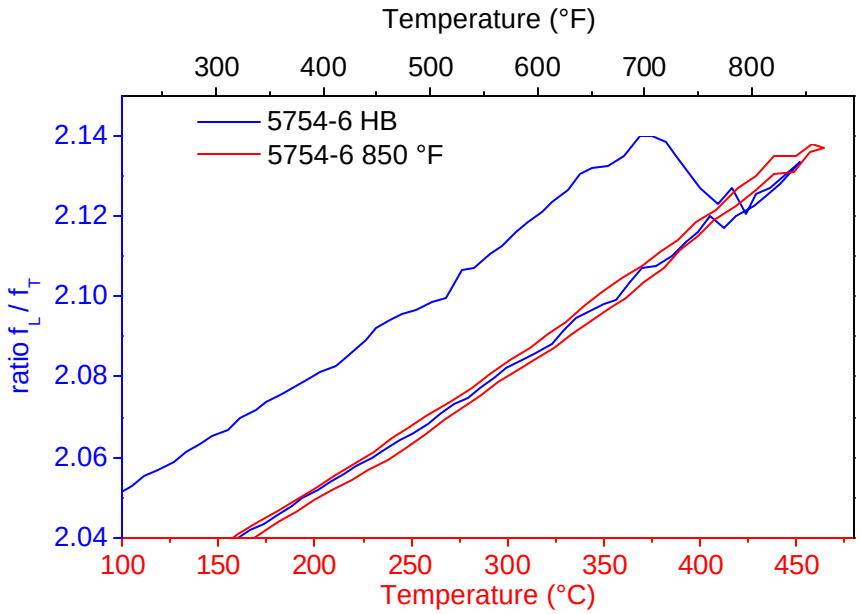


**Figure 32.** *k* ratio versus temperature for coil 5754-6: hot band sample (5754-6 HB) and annealed sample (5754-6 850 °F).

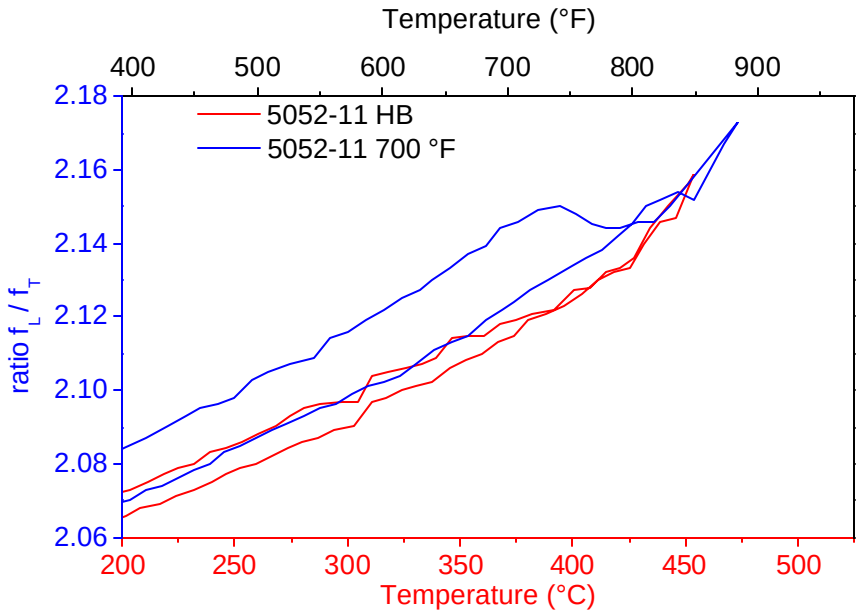


**Figure 33.** *k* ratio versus temperature for coil 5052-11: hot band sample (5052-11 HB) and annealed sample (5052-11 700 °F).

It is also interesting to note that improvements to our measurement technique allowed us to see the shear resonances to temperatures up to 450 °C, i.e. up to temperatures approximately

70 °C (126 °F) higher than those achieved before we built the prototype and with the prototype. In retrospect, it appears that the large improvements in signal to noise ratio that we obtained at room temperature through various procedures were not optimal at high temperatures. Future work should reconsider signal to noise optimisation at high temperatures.

In Figures 34 and 35, the $k$ ratios measured inline and in the laboratory are superimposed. Although the overall behavior is the same for both measurements, there are several differences. The temperature where the recrystallization begins is higher in the laboratory. The value of $k$ at which recrystallization begins is higher for the inline measurements. The drop in $k$ during recrystallization in the laboratory is about 0.02, as observed once inline but double what was observed in the others cases. Many factors may explain these discrepancies: the temperature drop between the inline furnace and the LUS measurement location, temperature measurement errors from the inline pyrometer, different temperature histories of the samples leading to different starting microstructures and amounts of stored energy, and different heating rates of the induction furnace and of the Gleeble. This discussion will now address these factors.

First, as it has been explained at length, the inline temperature measurement is not reliable. The pyrometer was calibrated near 450 °C (850 °F) on the alloy 5754. For this alloy, the temperature at which recrystallization begins is approximately the same inline and in the laboratory (380 °C inline near the furnace and 360 °C inline near the LUS measurement location, vs. 370 °C in the laboratory). On the other hand, for alloy 5052, there is a large discrepancy (350 °C inline near the furnace and 325 °C inline near the LUS measurement location, vs. 390 °C in the laboratory). In all likelihood, the emissivity of the two alloys is not the same and the IR camera temperature measurement for the alloy 5052 may be subject to large errors. To verify if this is the case, we note that the sharp increase in the ultrasonic attenuation above 500 °C (932 °F) seen in Figure 36 may be used as a means to test the calibration of the camera. It was found, in the laboratory, that this sharp increase in attenuation is the same for both grades and independent of recrystallization. Therefore, if two coils have the same attenuation, they must be at the same temperature. However, inline measurements of attenuation show that at constant attenuation, the IR camera temperature reading is systematically 50 °C (90 °F) lower for the alloy 5052 (Figure 36). Therefore, we must conclude that for the alloy 5052, recrystallization did not begin near 350 °C near the exit of the furnace, but near 400 °C, and in agreement with the laboratory measurements.

The reason why recrystallization begins at a higher value of $k$ inline is more difficult to explain. Assuming that these discrepancies do not result from systematic experimental errors (which we would not know how to explain), the simplest explanation is that the beginning texture of the coils is not the same as that of the hot band samples. The hot band samples were cut from the hot band with the shear that follows the hot rolling mill. They were air cooled from a hot band temperature of approximately 300 °C (575 °F) to room temperature.[6] On the other hand, the inline coils came directly from the hot rolling mill. Before the induction furnace, it is estimated that the coil temperature was down to approximately 290 °C (550 °F).[7] At the LUS measurement point, the lowest temperatures recorded by the IR camera on the alloy 5754 were approximately 250 °C (482 °F). Above 300 °C (575 °F), the temperature is high enough that some recrystallization may occur.[8] As the sheet moves from the hot rolling mill to the induction furnace, it is cooled by convection (as Figure 9 illustrates) at a faster rate than the hot band sample that was presumably left immobile while cooling. Therefore, it is not unreasonable to hypothesize that the hot band sample was partially recrystallized while the coil was not. This may explain why the hot band samples measured in our Gleeble had lower values of $k$ before recrystallization than the coils measured inline.

Finally, the drop in $k$ ratios observed inline appears to be less than that observed in the laboratory. This would seem to contradict the previous hypothesis because a higher initial $k$ ratio should lead to a larger drop when recrystallization occurs. However, our measurements usually ended with the disappearance of the shear acoustic resonance and we have no reason to believe that we did observe the end of recrystallization. Therefore, it is not be surprising that the drops in $k$ observed inline are equal to or less than those observed in the laboratory.

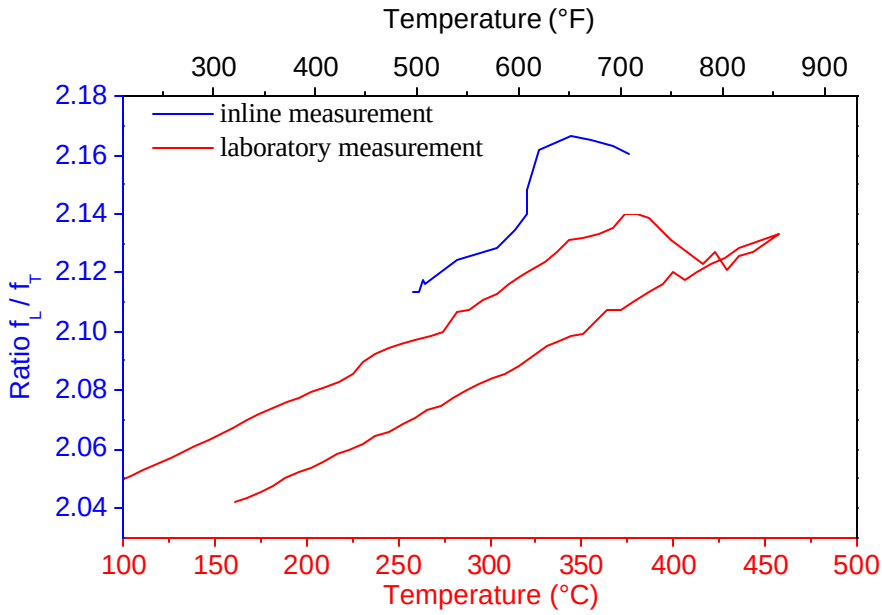


**Figure 34:** $k$ ratio versus temperature for the hot band sample 5754-6 HB, as measured in the laboratory, and for coil 5754-2, as measured inline.

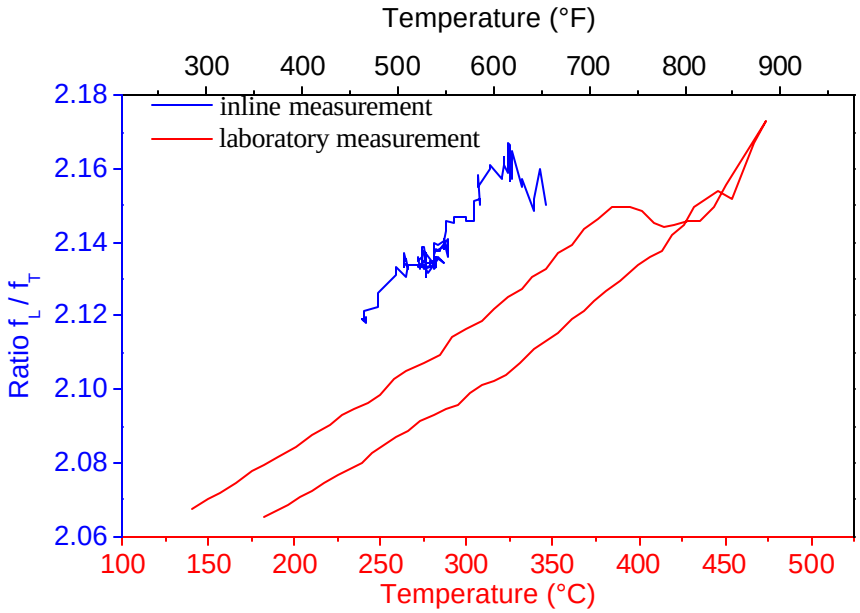


**Figure 35:** *k* ratio versus temperature for the hot band sample 5052-11 HB, as measured in the laboratory, and for coil 5052-13, as measured inline.

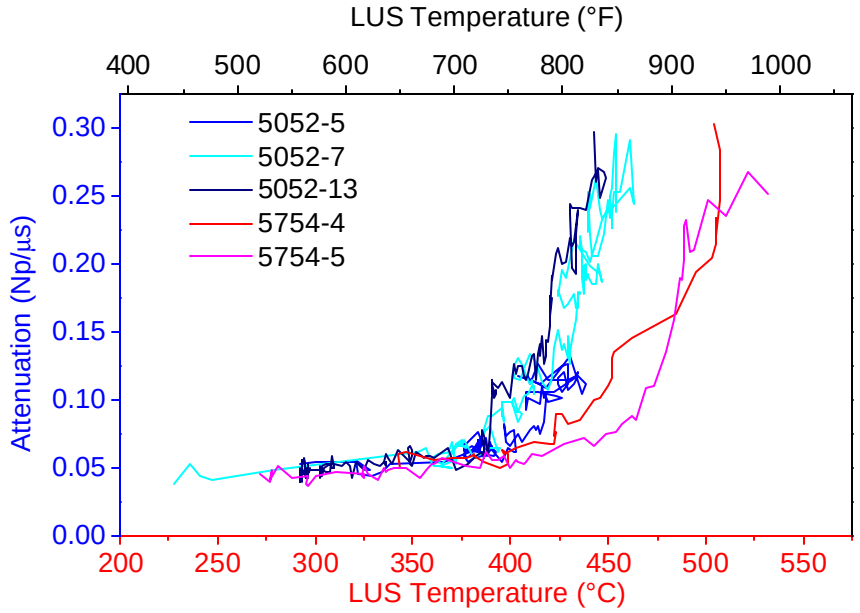


**Figure 36:** Attenuation of longitudinal waves versus temperature for the aluminum grades 5754 and 5052: inline measurements.

**Laser-ultrasonic attenuation and recrystallization**

The original goal of the project was to measure recrystallization by monitoring $k$ as a function of temperature. Considerations regarding signal to noise issues have prompted us to look at ultrasonic attenuation as well. Taking this one step further, could there be a signature of recrystallization in the attenuation measurement? Inline, only the attenuation of the longitudinal signal can be measured, but it can be measured to higher temperatures than $k$.

Work made for some other internal IMI project has shown that recrystallization does indeed affect the attenuation. The attenuation of recrystallized aluminum is lower and this is most easily observed at lower temperatures. At high temperatures, the effect is not large enough to be measurable above the steep temperature dependence of attenuation. This is shown in Figure 37 where the attenuation versus temperature measured in the laboratory for sample 5052-11 HB (hot band sample, not annealed) is given during heating and cooling. In this figure, the $k$ ratio versus temperature is also shown. For temperatures below 375 °C (707 °F), the attenuation during cooling is lower than during heating. Below 375 °C, the metal is fully recrystallized during cooling while it had not started to recrystallize during heating. Note that, it is difficult to find a feature corresponding to the occurrence of recrystallization during heating. In Figure 30, when recrystallization occurs, a small drop in the attenuation may be observed before the exponential increasing. The small drop was observed several times inline and may be a recrystallization signature. However, this feature cannot be seen in Figure 37 and, if it does exist, it is too small to be used to assess the recrystallization state of the strip.

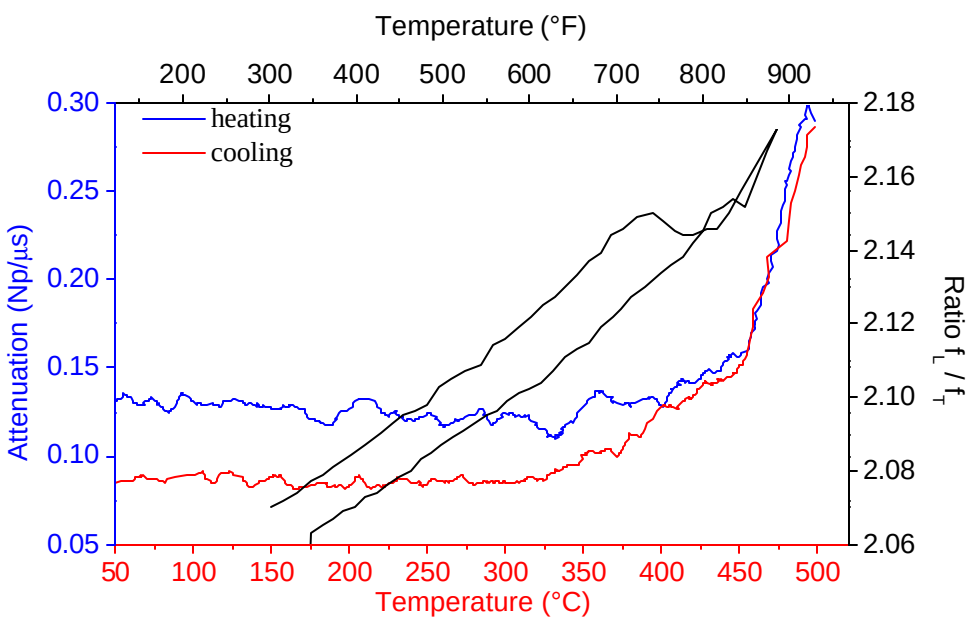


**Figure 37.** Attenuation of longitudinal waves versus temperature and $k$ ratio measured in the laboratory for hot band sample 5052-11 HB.

**Using longitudinal resonances and a thickness gauge**

It was shown how the longitudinal resonances are very sensitive to thickness variations. However, if one were to measure thickness with an accurate thickness gauge, using perhaps and x-ray gauge, could this resonance be used to measure recrystallization at higher temperatures that with $k$ ?

In Figure 38, the fundamental longitudinal frequency versus temperature measured in the laboratory is shown for the hot band sample 5754-6 HB and the annealed sample 5754-6 850 °F. Note that the two samples did not have the same thickness and that it was necessary to divide the fundamental longitudinal frequency of the annealed sample (5754-6 850 °F) by the ratio of thicknesses of the two samples to superimpose the cooling curves. For these samples, the $k$ ratio versus temperature is shown in Figure 32.

In Figure 38, for the hot band sample (5754-6 HB), the results obtained during heating are shown with a dotted line and during cooling with a straight line. For the annealed sample (5754-6 850 °F), the results obtained during heating and cooling are shown with a straight line since they are superimposed. As shown in Figure 32, the hot band sample recrystallizes at temperatures above 375 °C (707 °F) and the sample is fully recrystallized for temperatures above 400 °C (752 °F) and during cooling. The annealed sample was fully recrystallized before the measurements began. As shown in Figure 38, for the hot band sample during heating, the rate of change of the longitudinal fundamental frequency with temperature varies when recrystallization occurs. Moreover, the temperature of the longitudinal resonance frequency during cooling is superimposed to that of the inline-annealed samples, as expected since both are fully recrystallized.

However, the effect of recrystallization on the longitudinal resonance frequency is small and the $k$ ratio versus temperature curve gives clearer recrystallization signatures. For inline measurements, longitudinal velocity measurements could be obtained precisely up to very high temperatures provided that an equally precise thickness gauge is installed. The measured longitudinal velocity variations due to recrystallization are 0.6 % and 0.3 % for the grade 5754 and 5052, respectively. Consequently, a thickness measurement with a precision of 0.1 % or better would be necessary.

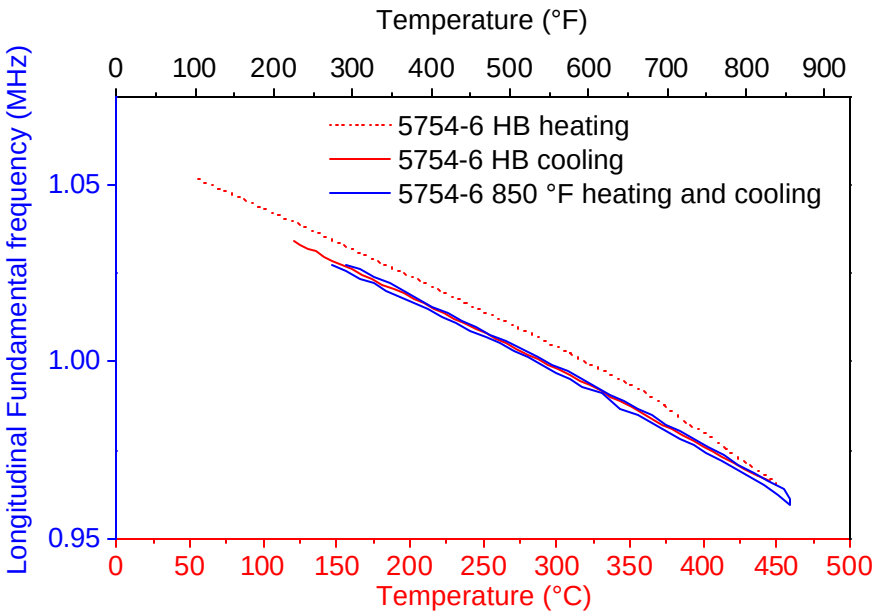


**Figure 38.** Longitudinal fundamental frequency versus temperature measured in the laboratory for the hot band sample 5754-6 HB and the annealed sample 5754-6 850 °F.

## *IV Practical considerations for inline LURS measurement of recrystallization*

### Introduction

Inline induction annealing of aluminum strips has potentially many advantages as compared to batch annealing. It should greatly simplify processing of annealed products and logistics around the plant. It should offer substantial reduction in energy consumption because it takes the hot band material directly to annealing temperature, as opposed to material that has cooled to room temperature. It should produce strips with more uniform properties between the front, middle and end of the coil.

The addition of inline sensing of recrystallization after inline annealing may render inline annealing even more attractive. It may help further reduce energy consumption by monitoring the exact moment at which recrystallization is achieved and thus avoid over-annealing for the purpose of ensuring a “safety margin”. It provides instantaneous quality control along the full length of the coil. And it may be used for immediate feedback on the processing equipment, thus greatly reducing setup time between different grades or allowing to take immediate action when some particular process parameters drifts out of its normal operating range. This could help greatly reduce the amount of scrap and return shipments from dissatisfied customers. This section of the report suggests various ways in which the laser-ultrasonic sensor developed in this project could be used inline for these purposes.

### Limitations of inline annealing

The dependence of the recrystallization fraction, $X$, as a function of annealing time, $t$, and temperature, $T$, is described by the well-known JMAK model whereby

$$X = 1 - \exp(-bt^n) \quad \text{and} \quad b = A \exp(-Q/RT) \,. \qquad (2)$$

Here, $n$ is the JMAK exponent, $A$ is a constant, and $Q$ is the activation energy for recrystallization.[9] The three parameters depend on alloy chemistry grade, amount of cold work, and previous thermal history. Therefore, no single set of model parameters is available to cover the production range of a mill. In addition, the strip temperature varies with the amount of cold work in the rolling mills and with continuous cooling everywhere else. Furthermore, the cooling rate of the strip depends on strip thickness, line speed (because of convection cooling, see Figure 9), strip emissivity (radiative cooling), etc... Therefore, it is quite difficult to accurately model the recrystallization state of an aluminum strip.

To fully anneal a strip, one must insure that temperature is high enough and that time is long enough. This is usually achieved by a process of trial and error and by building a database of processing information. However, each time process parameters move outside of the recorded data base, one risks under annealing the strip. And because fully recording all process variables and all corresponding microstructures for all grades produced would be exceedingly expensive, one tends to over anneal the strip somewhat either by increasing the annealing temperature or by increasing the holding time at that temperature.
Another difficulty with inline annealing of aluminum is that the temperature of the strip is difficult to measure. One begins to appreciate this by reading Section II of this report and by noticing the

large effort we had to provide to obtain only approximate temperature readings. Again, a simple solution is to increase annealing temperature somewhat to compensate for temperature measurement error. However, over annealing increases energy consumption and costs.

## Inline monitoring of the recrystallized fraction

In contrast with over annealing the strip to compensate for the shortcomings of the inline annealing process, inline monitoring of the recrystallized fraction offers the possibility to feed back on annealing temperature so that it may be just high enough to attain the full recrystallization. Thus additional energy savings may be possible.

It must be emphasized that inline monitoring of the recrystallized fraction is completely independent of all process parameters. It is a reading of the current microstructure of the strip at one specific location. This reading may be extremely valuable in instantaneously assessing whether the line is operating according to expectations. Used as a quality control tool, inline monitoring of the recrystallization may allow to immediately detect production anomalies resulting from the drift or control loss of some process variable.

### *Monitoring with an established calibration*

The laser-ultrasonic measurement of $k$ may be used in two ways to measure the recrystallization state of the strip. As suggested earlier in this report, one may build a calibration curve of $k$ vs. temperature for the hot band and recrystallized material as a function of temperature (see Figures 32 and 33 for examples). Once the calibration curve is made for a specific alloy and processing route, the recrystallization state of the strip may be assessed by measuring $k$ and temperature.

### *Monitoring with no established calibration*

If no such calibration curve is available perhaps because some alloy is being produced for the first time, one may simply monitor $k$ as temperature is raised gradually. If above some temperature, $k$ suddenly departs from smooth temperature dependence, then this is a signature that texture changes and that recrystallization occurs. In this report, this showed up near furnace temperatures of 380 °C (716 °F) as a drop in $k$ with temperature. This method is the one we used for the inline tests that we report herein because no reliable calibration curve was available (alloy 5052 had never been tested and alloy 5754 was tested with material which had followed a processing route unknown to us). If recorded, this data could be used to build a new calibration curve, inline, without the need for further laboratory measurements. Figures 28 and 29 are initial results towards such an inline calibration. The recorded data could also be used to augment the plant's database on the influence of process parameters on the recrystallization state of the strip.

## Limitations of inline monitoring of the recrystallized fraction:

### *Temperature measurement*

Because $k$ varies simultaneously with temperature and texture, a measurement of temperature is essential to obtain the texture information. However, inline measurement of temperature of

aluminum strips is difficult. This report unequivocally demonstrates that a single color pyrometer is inadequate. Within the scope of this project, it is not possible to recommend a specific pyrometer, although we expect that there should be a few suitable choices.

*Maximum operating temperature*

The maximum temperature at which the sensor operates properly is approximately 380 °C (716 °F). Further laser-ultrasonic developments could raise this limitation. In particular, recent laboratory measurements hint that temperatures of up to 450 °C (842 °F) might be achievable, although more work is required to confirm this. The 380 °C maximum temperature was just high enough to measure recrystallization. During the tests reported herein, the sensor could sense the onset of recrystallization but could not sense beyond full recrystallization. However, these tests were made in conditions that were probably more demanding than what normal production conditions would be: The induction furnace heating power was ramped up very quickly and data averaging could only be made over a short time interval of order one second; the sensor was located near the induction furnace which resulted in very little time (4 seconds) for recrystallization to happen; and finally, strip thickness was larger than what the sensor had been designed for.

It must be noted, however, that the longitudinal resonance were observed to temperatures as high as about 460 °C (860 °F). If a thickness gauge accurate to ± 0.1% were used with the LURS sensors, recrystallization could possibly be sensed up to 460 °C.

*Different calibrations for different alloys having different hot rolling and annealed texture*

The inline annealing sensor senses $k$, a parameter representative of the strip texture. Alloys and processing routes causing different initial and final textures will require different calibrations. However, it was discussed earlier how these calibrations might be obtained inline.

*Strip thickness*

Laser-ultrasound spectroscopy was developed to sense thin strip material. The thinner the strip is, the better the technique works. Most laboratory measurements were made with samples of order 1 mm thick. We have never tested what is minimum measurable strip thickness, but strips 100 microns thick should be relatively easy to measure. The strips measured inline at CAC were approximately 4 mm thick and relatively difficult to measure. Above some thickness, we expect that a technique based on time of flight measurements would offer more accurate results. This would require new data analysis algorithms but it would not require new laser-ultrasonic hardware.

*Strip marking*

The laser used to generate the ultrasound leaves a discoloration on the surface of the strip. The aluminum appears shinier, as if its surface had been cleaned. No measurable loss of thickness is observed, even if many laser shots are made on the same spot (inline, each time the laser fires, it fires on a new location on the strip because the strip moves). The surface mark is not expected to affect the mechanical properties of the strip. As far as we know, it is purely a

cosmetic issue (even if these issues may be extremely important, sometimes). Solutions to this limitation (other than having the customer accept the mark as a proof of inline inspection and quality control!) are to limit the inline measurements to the edges of the strip and using an edge trimmer, to limit the inline measurement to front and tail ends of coils, to limit the inline measurement to products where surface appearance is not an issue.

IMI is currently developing another generation laser that might eliminate this problem altogether.

## Designing a processing line that includes a LUS sensor

In this section, we comment on the usefulness and suitability of the LUS sensor for several processing line configurations.

*Hot rolling, inline annealing, sensing, coiling*

A processing line consisting of hot rolling, inline annealing, LUS sensing, and coiling would be cheapest and would realize many of the benefits of inline annealing. In such a configuration, the cooling rate of the coil is so slow that it is cost effective to run the annealing furnace at a relatively low temperature, whereby recrystallization happens very slowly, inside the coil. The JMAK model predicts that recrystallization is a rather sudden process, with a relatively long pre-recrystallization time when nothing happens. The LUS sensor would sense during pre-recrystallization and would be useless.

This configuration would have the lowest energy consumption but would retain many of the problems associated with batch annealing. Because the coil would have a non-uniform temperature distribution during coiling and cooling, the strip properties may not be uniform.

*Hot rolling, inline annealing, coiling, sensing on a separate inspection line*

To diagnose possible non-uniformity problems with the previous configuration, some or all of the coils produced could be inspected on a separate inspection line. The LUS measurements would be made at room temperature. They would be simpler, more precise, more reliable, and possibly cheaper. The LUS sensor would be a quality assurance tool.

*Hot rolling, inline annealing, holding, sensing, quenching, coiling*

To improve product uniformity, it would be better to anneal for some time at some temperature and then quench the strip. The strip does not need to be quenched to room temperature, but only by approximately 50 °C (90 °F) because every drop in temperature by 25 °C (45 °F) increases annealing time by a factor of 10. Other heat treatment processing may also be considered after quenching, such as holding at some intermediate temperature to obtain precipitation hardening.

To minimize energy consumption, one might build an enclosure to minimize strip cooling after the induction furnace. The strip would remain for a longer time at its highest temperature thus improving recrystallization kinetics or, conversely, allowing to further reduce the annealing temperature. At the end of the holding period, the strip would be sensed and quenched. Because of the holding time would be much longer than the 4 seconds we had during the tests

at CAC, the strip temperature should be lower (by perhaps 25 °C for a holding time of 40 seconds) and the sensor should work even better.

*Hot rolling, inline annealing, holding, quenching, sensing, coiling*

Inline sensing of recrystallization does not have to be done at high temperature. A variation on the previous configuration would be to sense the recrystallization state of the strip after quenching. Assuming that quenching is made with water, an air knife or some other device would be required to remove the excess water on the strip surface. Also, the strip should be allowed to equilibrate in temperature before the LUS measurements to avoid errors in temperature readings. Because the measurements would be made at much lower temperatures than 380 °C (716 °F), the LUS sensor should have a much better signal to noise ratio than during the inline tests at CAC.

## Other benefits

*Annealing a new grade*

As discussed previously, when a new grade is introduced to the processing line, the inline annealing furnace temperature may be slowly ramped up until a sudden change in $k$ is observed, indicating that recrystallization has occurred. This procedure would minimize setup time and decrease the amount of scrap produced when there is a grade change or when a new alloy is made for the first time. In this application, there is no need for accurate pyrometry.

*Thickness measurements*

In addition to demonstrating how the LUS sensor can measure recrystallization and texture, it was also shown how it can measure strip thickness. Variations of order 1% were easily monitored. Based on previous work, the expected measurement precision should be of order 0.1%.

## Total savings

This section of the report has described how various savings could be made with laser-ultrasonic inline monitoring of the recrystallized fraction. To make this analysis quantitative, proprietary data is required. We hope that enough information has been given so that the industrial engineer who has access to this proprietary data may prove the economic value of the sensor.

## *V Conclusion*

### Recalling the objectives

The goal of this project was to determine whether 1) aluminum sheets can be fully recrystallized using an induction furnace after hot rolling and whether 2) recrystallization can be monitored inline with a laser-ultrasonic sensor. We can now safely conclude that the alloys 5754 and 5052 did begin to recrystallize inline approximately four seconds after being heated to 380 °C (716 °F). This was observed using a laser-ultrasound system based on resonance spectroscopy. The sensor operated successfully inline to temperatures up to 380 °C (716 °F). Clearly, the project is a scientific success. Will the project be an economic success as well? This question can only be answered with an economic analysis. But some of the potential benefits were identified qualitatively in this report.

### The future

The prototype tested at CAC was assembled from laboratory components. It was not designed to operate unattended, it was over-designed, and it would not survive for long periods of time. The prototype was intended and designed to prove the principle of the inline recrystallization measurement at the lowest cost. The next step is to design and build the first commercial-like system. This might take one year or more from the time a contract is awarded. The commercial-like system would cost between 0.5 to 1 million U.S. dollars. The system would be installed at some permanent location and run for some extended time. Minor modifications might be made as we learn how to use it to its full potential. Perhaps one year after it is installed, it could be fully commercialized.

This commercialization path would be similar to what is currently happening at The Timken Company, where a full-scale, commercial-like system has been running in production for the past year.[10] This system measures the wall thickness and eccentricity of seamless tubing at high temperatures (approximately 1000 °C), as well as tube temperature and position along the length and circumference. Several hundred thousand tubes have been measured and the system is now an integral part of the production system. Apparently, the economic benefits far outweigh the instrument cost.

## *VI Appendix I – Basic data for samples taken inline at CAC*

**Table I.** Samples from In-Line Anneal Trials at Carson Rolling Mill. The temperatures are the maximum values measured using a contact thermocouple. Mill speeds for the 5052-X samples are approximate.

| Coil ID | Gauge (inch) | Temperature (°F) | Temperature (°C) | Mill speed (feet/min) | Mill speed (m/s) | Coil |
|---|---|---|---|---|---|---|
| 5754-1 | 0.160 | 750 | 399 | 114 | 0.58 | Yes |
| 5754-2 | 0.160 | 800 | 427 | 116 | 0.59 | Yes |
| 5754-3 | 0.160 | 875 | 468 | 114 | 0.58 | Yes |
| 5754-4 | 0.160 | 950 | 510 | 113 | 0.57 | Yes |
| 5754-5 | 0.160 | 1000 | 538 | n.a. | n.a. | Yes (Melt) |
| 5754-6 | 0.120 | 850 | 454 | 145 | 0.74 | Yes (Melt) |
| 5052-1 | 0.120 | 750 | 399 | 152 | 0.77 | Yes |
| 5052-2 | 0.120 | 800 | 427 | 152 | 0.77 | Yes |
| 5052-3 | 0.120 | 875 | 468 | 152 | 0.77 | Yes |
| 5052-4 | 0.120 | 850-880 | 454-471 | 152 | 0.77 | Yes (Melt at 875) |
| 5052-5 | 0.160 | 750 | 399 | 114 | 0.58 | Yes |
| 5052-6 | 0.160 | 810 | 432 | 114 | 0.58 | Yes |
| 5052-7 | 0.160 | 720 | 382 | 114 | 0.58 | Yes |
| 5052-8 | 0.160 | 650 | 343 | 114 | 0.58 | Yes |
| 5052-9 | 0.160 | 850 | 454 | 114 | 0.58 | Yes |
| 5052-10 | 0.084 | 650 | 343 | 217 | 1.55 | Yes |
| 5052-11 | 0.084 | 700 | 371 | 217 | 1.55 | Yes |
| 5052-12 | 0.084 | 775 | 413 | 217 | 1.55 | Yes |
| 5052-13 | 0.084 | 850 | 454 | 217 | 1.55 | Yes (Melt) |

## *VII Appendix II – X-ray texture data for samples taken inline at CAC*

**Table II** Texture coefficient measured using x-ray diffraction by C.-S. Man of the University of Kentucky. WQ refers to water quenched samples.

| Sample | Position | Layer | $W_{400} \times 10^2$ | $W_{420} \times 10^2$ |
|---|---|---|---|---|
| 5052-6 810F WQ | Center | Surface | 0.4254 | -0.1576 |
| | | Quarter | 0.6049 | -0.06295 |
| | | Center | 0.6678 | -0.07452 |
| | Edge | Surface | 0.3636 | -0.1210 |
| | | Quarter | 0.5788 | -0.05734 |
| | | Center | 0.6039 | -0.05354 |
| 5052-8 650F WQ | Center | Surface | 0.2760 | -0.2636 |
| | | Quarter | 0.1321 | -0.04414 |
| | | Center | -0.0453 | -0.1835 |
| | Edge | Surface | 0.1332 | -0.1636 |
| | | Quarter | -0.0620 | -0.1971 |
| | | Center | 0.00192 | -0.1366 |
| 5052-11 775F WQ | Center | Surface | 0.5298 | -0.09269 |
| | | Quarter | 0.8016 | -0.1621 |
| | | Center | 0.7604 | -0.1739 |
| | Edge | Surface | 0.5167 | -0.1724 |
| | | Quarter | 0.6476 | -0.1492 |
| | | Center | 0.7081 | -0.1495 |
| 5754-3 740F WQ | Center | Surface | 0.2957 | -0.2306 |
| | | Quarter | 0.6326 | -0.1563 |
| | | Center | 0.7234 | -0.1818 |
| | Edge | Surface | 0.3795 | -0.1322 |
| | | Quarter | 0.6304 | -0.1671 |
| | | Center | 0.6634 | -0.1583 |
| 5754-5 1040F WQ | Center | Surface | 0.4095 | -0.2081 |
| | | Quarter | 0.6861 | -0.1309 |
| | | Center | 0.8312 | -0.1013 |
| | Edge | Surface | 0.4986 | -0.1871 |

| | | | | |
|---|---|---|---|---|
| | | Quarter | 0.7436 | -0.08328 |
| | | Center | 0.8123 | -0.04358 |

| Sample | Position | Layer | $W_{400} \times 10^2$ | $W_{420} \times 10^2$ |
|---|---|---|---|---|
| 5052-3-1 HB | Center | Surface | -0.1042 | -0.1578 |
| | | Quarter | -0.1567 | -0.1507 |
| | | Center | -0.1543 | -0.1484 |
| | Edge | Surface | 0.1138 | -0.1409 |
| | | Quarter | 0.001863 | -0.03823 |
| | | Center | -0.1956 | -0.3037 |
| 5052-6-1 HB | Center | Surface | 0.1271 | -0.06961 |
| | | Quarter | 0.1113 | -0.01067 |
| | | Center | 0.01632 | -0.1886 |
| | Edge | Surface | -0.03919 | -0.1202 |
| | | Quarter | 0.02093 | -0.1569 |
| | | Center | -0.0003828 | -0.09009 |
| 5754-2-1 HB | Center | Surface | 0.1491 | -0.1882 |
| | | Quarter | 0.1551 | -0.08804 |
| | | Center | -0.08910 | -0.1447 |
| | Edge | Surface | 0.1118 | -0.1605 |
| | | Quarter | 0.09803 | -0.3300 |
| | | Center | -0.06934 | -0.1858 |
| 5052-11 HB | Center | Surface | 0.4779 | -0.2075 |
| | | Quarter | 0.1644 | -0.09919 |
| | | Center | 0.07398 | -0.1141 |
| | Edge | Surface | 0.05588 | -0.2266 |
| | | Quarter | 0.01598 | -0.08912 |
| 5754-6-1 HB | Center | Surface | 0.2472 | -0.1785 |
| | | Quarter | 0.4591 | -0.1231 |
| | | Center | 0.01252 | -0.1691 |
| | Edge | Surface | 0.1492 | -0.1599 |
| | | Quarter | 0.008127 | -0.2026 |

| Sample | Position | Layer | $W_{400} \times 10^2$ | $W_{420} \times 10^2$ |
|---|---|---|---|---|
| 5052-1 750F | Center | Surface | 0.3052 | -0.08465 |
| | | Quarter | | |
| | | Center | | |
| 5052-2 800F | Center | Surface | 0.5671 | -0.1164 |
| | | Quarter | | |
| | | Center | | |
| 5052-3-2 875F | Center | Surface | 0.4578 | -0.1258 |
| | | Quarter | | |
| | | Center | | |
| 5052-4 850F-880F | Center | Surface | 0.5743 | -0.08878 |
| | | Quarter | | |
| | | Center | | |
| 5052-5 750F | Center | Surface | 0.4696 | -0.1368 |
| | | Quarter | | |
| | | Center | | |
| 5052-6-2 810F | Center | Surface | 0.5007 | -0.1263 |
| | | Quarter | | |
| | | Center | | |
| 5052-7 720F | Center | Surface | 0.4730 | -0.07651 |
| | | Quarter | | |
| | | Center | | |

## *VIII Appendix III – Suppliers of laser-ultrasonic equipment.*

IMI is a government laboratory whose purpose is to conduct research in various fields of materials processing. IMI does not intend to manufacture commercial equipment although it may contribute as required. IMI has licensed parts of its laser-ultrasound technology to the following two firms:

Tecnar Automation
1321 Hocquart
Saint-Bruno, QC
Canada J3V 6B5
http://www.tecnar.com/

Ultra-Optec
4815 Chemin de la Savane
Saint-Hubert, QC
Canada J3Y 9G1
http://www.ultraoptec.com/

## *IX References*

**1.** André Moreau, Teodor Veres, Silvio E. Kruger, Martin Lord, Stéphane Bolognini, Christophe Bescond. "Laser-Ultrasound Resonance Spectroscopy Measurement of Texture in Aluminum, A compilation of reports produced under Subcontract 4-63800-00-305 between UKRF and NRC" Produced for University of Kentucky Research Foundation, Lexington KY. *Industrial Materials Institute*, #IMI 2003-98917-C, 2003, 28 pages.

André Moreau, Stéphane Bolognini, Christophe Bescond, Martin Lord, Silvio Kruger. "In-line Monitoring of Texture in Strip-Cast Aluminum Alloys using Laser-Ultrasound Resonance Spectroscopy – Annual Report, May 1 2001 to April 5 2002" Produced for University of Kentucky Research Foundation, Lexington KY. Industrial Materials Institute, #IMI 2002-93994-C, 2002, 6 pages.

**2.** D. Lévesque, A. Moreau, M. Lord, M. Dubois, J.-P. Monchalin, C. Padioleau, and J. F. Bussière. "On-line Measurement of Texture, Thickness, and Plastic Strain Ratio on Steel Sheets Using Laser-Ultrasound Resonance Spectroscopy." *Advanced Sensors for Metals Processing*. Proceedings of the International Symposium on Advanced Sensors for Metals Processing, Quebec City, Canada, 22-26 August 1999. Edited by B. W. Brusey, J. F. Bussière, M. Dubois, and A. Moreau. Canadian Institute of Mining, Metallurgy and Petroleum, Montreal, 1999. p. 53-65.

A. Moreau, D. Lévesque, M. Lord, M. Dubois, J.-P. Monchalin, C. Padioleau, and J. F. Bussière. "On-line Measurement of Texture and Plastic Strain Ratio on Steel Sheets Using Laser-Ultrasonics." *Proceedings of the Twelfth International Conference on Textures of Materials*, Montreal, Canada, 9-13 August 1999. Edited by Jerzy A. Szpunar (NRC Research Press, Ottawa, 1999). p. 493-498.

D. Lévesque, A. Moreau, M. Lord, M. Dubois, J.-P. Monchalin, C. Padioleau, and J. F. Bussière. "On-line Measurement of Texture, Thickness, and Plastic Strain Ratio on Steel Sheets Using Laser-Ultrasound Resonance Spectroscopy." *Advanced Sensors for Metals Processing*. Proceedings of the International Symposium on Advanced Sensors for Metals Processing, Quebec City, Canada, 22-26 August 1999. Edited by B. W. Brusey, J. F. Bussière, M. Dubois, and A. Moreau. Canadian Institute of Mining, Metallurgy and Petroleum, Montreal, 1999. p. 53-65.

A. Moreau, D. Lévesque, M. Lord, M. Dubois, J.-P. Monchalin, C. Padioleau, and J. F. Bussière. "On-line Measurement of Texture and Plastic Strain Ratio on Steel Sheets Using Laser-Ultrasonics." *Proceedings of the Twelfth International Conference on Textures of Materials*, Montreal, Canada, 9-13 August 1999. Edited by Jerzy A. Szpunar (NRC Research Press, Ottawa, 1999). p. 493-498.

**3.** A. Moreau. "Safety Assessment Report Concerning the Laser-Ultrasonic Prototype to be Installed at Commonwealth Aluminum Corporation in Carson" Produced for Commonwealth Aluminum Corporation, Uhrichsville, OH. Industrial Materials Institute, #IMI2002-9480-C 2002, 31 pages.

**4.** C.-S. Man, X. Fan, J.C. Morris and K. Kawashima. "Monitoring of Primary Recrystallization in Aluminum Alloy by Resonance EMAT Spectroscopy", Proceedings of the 13th International Conference on Textures of Materials, Seoul, Korea, August 2002, Edited by D. N. Lee, Published in Textures of Materials**,** Trans Tech Publications, 2002, pp.875-880.

**5.** Silvio E. Kruger, André Moreau, Matthias Militzer, and Taryn Biggs. “Monitoring the Annealing of an Al-Mg Alloy by Laser-ultrasonics.” *Light Metals 2002 Métaux Légers.* Proceedings for the 2002 Light Metals Symposium of the Conference of Metallurgists of the CIM, Montreal, Canada, 11-15 August 2002. Edited by T. Lewis. Canadian Institute of Mining, Metallurgy and Petroleum, Montreal, 2002. p. 161-171.

**6.** Zhong Li, private discussion. This temperature is a rough estimate.

**7.** Zhong Li, private discussion. This temperature is a rough estimate.

**8.** S.E Kruger et al., *op. cit*.

**9.** T. Furu, K. Marthinsen, and E. Nes. “Modeling recrystallization”. Materials Science and Technology, Vol. 6 (November 1990) 1093-1102.

**10.** J.-P. Monchalin, M. Choquet, C. Padioleau, C. Néron, D. Lévesque, A. Blouin, C. Corbeil, R. Talbot, A. Bendada, M. Lamontagne, R. V. Kolarik II, G. V. Jeskey, E. D. Donimik, L. J. Duly, K. J. Samblanet, S. E. Agger, K. J. Roush, M. L. Mester. “Laser ultrasonic system for on-line steel tube gauging” *Review of Progress in Quantitative Nondestructive Evaluation* Vol. 23 (2003), in press.